Journal of Building Engineering 113 (2025) 114060

Contents lists available at ScienceDirect

Journal of Building Engineering

journal homepage: www.elsevier.com/locate/jobe

Characterization of 3D printed concrete mixtures developed using local UAE materials based on rheological properties

Reem Sabouni [a,*], Samer Al Martini [a,b]

[a] Civil Engineering at Department of Civil Engineering, College of Engineering, Abu Dhabi University, Abu Dhabi, 59911, United Arab Emirates
[b] Affiliate Faculty, University of British Columbia (UBC), Canada

ARTICLE INFO

Keywords:
3D printing concrete
Rheology
Dynamic yield stress
Slump flow

ABSTRACT

This paper investigates the fresh and rheological properties of 3D printed concrete mixes developed using locally available United Arab Emirates (UAE) materials. Thirty-two 3D printed concrete mixes were developed with various constituents. These constituents included: water to binder ratio (w/b), superplasticizer (SP), fly ash (FA), silica fume (SF), and two types of fibers: Stewathix 600 (ST600) fiber and Glass Short Cut - FGCS HP (HP6) fiber. A rating procedure was developed to qualitatively and quantitatively evaluate and rate the printability of 3D concrete mixes. This evaluation procedure employs a manual mortar gun that is suitable to be used for on-site assessment. Also, a printability chart relating dynamic yield stress to plastic viscosity was developed. A recommended printability box was identified suggesting that 3DPC mixes with plastic viscosity between 15 and 97 Pa.s and dynamic yield stress between 400 and 1500 Pa are likely to demonstrate adequate printability. This chart can aid in the design and quality control of 3D printing concrete mixes. The open time test was performed on four selected mixes. The results revealed that medium dosages of ST600 (0.11 %–0.22 %) and HP6 (0.15 %–0.22 %) fibers enhanced the extrudability of 3DPC mixes, while contributing to a reduction in flowability. These mixes fell within the defined printability box. A lower w/b ratio enhanced short-term printability, whereas a higher ratio was needed for longer durations. Microsilica improved early printability but led to reduced performance after 1 h. Finally, a large-scale laboratory printer was used to evaluate the printability of selected 3DPC mixes that fell within the identified printability box. The paper presents valuable practical insights for the construction industry in the UAE, which can foster the adoption of this technology in construction.

1. Introduction

Conventional construction involves intensive labor activities required for concrete mixing, formwork and concrete casting [1]. It is crucial to implement sustainable construction methods that can reduce the number of required workers at construction sites and eliminate the use of formwork. Construction using 3D concrete printing technology can serve as a suitable construction method to meet these requirements, as it can decrease the number of labors [2]. It can also help mitigate the environmental impact on construction sites by reducing the excessive use of wooden formwork, minimizing waste from rejected low-quality concrete, and lowering dust generation associated with traditional construction practices. [3]. The adoption of such emerging technology has the potential to

* Corresponding author.
E-mail addresses: reem.sabouni@adu.ac.ae (R. Sabouni), samer.almartini@adu.ac.ae (S. Al Martini).

https://doi.org/10.1016/j.jobe.2025.114060
Received 15 November 2024; Received in revised form 7 September 2025; Accepted 10 September 2025
Available online 11 September 2025

transform the construction sector, opening new horizons that demand specialized technical expertise and expanding the possibilities for innovative building design and architecture [4]. Compared to 3D printing construction, precast elements with many different geometries can result in over hundreds of different wooden molds that will be turned to waste after the completion of a specific project [5–7]. Also, molding and demolding involve a significant number of man-hours, and subsequently, higher labor costs [3]. This shows that one of the main challenges of traditional concrete is related to the physical labor required for the in-situ placement process, particularly for bespoke geometries [8].

3D printed concrete is expected to become the favored material for construction, due to its efficiency, cost effectiveness and innovative potential [9]. When compared to conventional construction, 3D-printed concrete uses less energy and may be optimized for working circumstances. Widespread adoption and promotion of 3D-printed concrete technology can significantly reduce material consumption, labor requirements, and equipment usage, while accelerating the advancement of digital and intelligent construction practices [10,11].

As the 3D printed concrete is constructed without the support of formworks, obtaining adequate buildability is still an issue, in particular when more layers are printed, the bottom layers will suffer from the weight of the above layers. The buildability is influenced by the properties of the materials incorporated. It was reported elsewhere [12] that the incorporation of recycled sand has improved the buildability of 3D printed layers [12]. The replacement of cement with mineral admixtures like fly ash, slag, and silica fume can improve the buildability of 3DPC and its mechanical performance [13,14].

The static yield stress has a direct impact on the buildability of 3DPC. In order to ensure good buildability, the static yield stress should be adequate [15]. The buildability of 3DPC is also affected by factors like early structuration and setting [16]. Deng Q et al. [17] reported that the replacement of cement with waste glass powder can improve buildability. The higher static yield stress results in more stable prints, as the relative deformation of the first layer decreases non-linearly. Further, several factors affect the deformation such as the interplay between extrusion pressure, cross-sectional shape, and contact area between layers [18,19].

The printability of 3D printing concrete (3DPC) is largely influenced by its rheological properties, which are affected by various factors including cement replacements, supplementary binder materials, superplasticizers, viscosity modifying agents, and the inclusion of fibers. The viscosity modifying agents like hydroxy propyl methyl cellulose (HPMC) were found to promote the printability of concrete [20]. For good and smooth extrudability and pumpability, the dynamic yield stress should be low [19,21]. If the dynamic yield stress is too high, it would make concrete difficult to extrude. Further, too high dynamic yield stress reduces the open time and consequently the printability window. The width and uniformity of the print strips are also affected by the rheological properties [22]. It was reported that steel fibers and nano-clay can improve the extrudability of 3DPC by increasing the dynamic yield stress, and apparent viscosity of 3DPC, [23]. The extrusion speed of printed strips shows a strong positive correlation with the material's plastic viscosity, indicating that rheological property testing can effectively guide the determination of optimal extrusion speed [24].

Researches on several advanced materials showed their potential to be incorporated in 3D printed concrete (3DPC) to improve extrusion stability, rheology, and printability. For example, the effect of the CaO/MgO ratio on phase formation ceramic tiles was investigated by Ref. [25]. The study showed that reducing this ratio increased anorthite formation, suppressed the undesirable gehlenite phase, and lowered the thermal expansion coefficient. These findings suggest that such materials could have the potential to enhance extrusion stability and dimensional control of 3DPC. Another study [26] used aluminum alkoxide derived from recycled aluminum through a sol–gel process to produce alumina. They found that aging conditions (80 °C, 24 h) and calcination at 900 °C optimized the surface area, porosity, and crystalline ordering, producing nanoparticles of 20–40 nm that assembled into porous structures suitable as catalyst supports. Such porous alumina materials, developed for catalytic applications, may hold potential for future 3D printed concrete (3DPC) research, where tailored surface area and porosity could enhance particle packing, extrusion behavior, and interlayer bonding.

Similarly, a study [27] used zirconium alkoxide and boric acid as precursors to produce ZrB_2 nanoparticles via the sol–gel method, with particle size controlled by pH and crystallization behavior influenced by temperature. With crystallization around 1500 °C, fine, uniform nanoparticles with porous surfaces and a high specific surface area (115 m^2/g) were achieved. Such nanostructured ZrB_2 materials used for ceramic production may hold potential to be incorporated in 3D printed concrete (3DPC), where their surface properties and stability could contribute to improved particle packing, extrusion control, and interlayer bonding. The integration of alternative binders such as geopolymers in 3D printed concrete (3DPC) can promote sustainability by reducing the carbon footprint. Geopolymer systems can enhance rheological control, extrusion consistency, and buildability in 3DPC applications [28].

Designing a proper 3D printing concrete mixture, while maintaining applicable rheological properties, is still a challenge. Other challenges of 3D printed concrete are: finding an appropriate pumping rate, overcoming the surface defects during printing of the consequent layers, inadequate cohesion between layers, and the printed layer's dimensional effect on the properties of concrete including its hardened strength [29,30]. It is noted by Ref. [30] that the printed layer with an oval shape negatively affects the adhesion zone between two consecutive layers, thus decreasing the bearing capacity of the printed structure. Some researchers investigated the fiber to mitigate the shrinkage of 3D printed concrete [31].

Although rheology and fresh-state properties play a critical role in 3D-printed concrete (3DPC), there are currently no standardized on-site tests to evaluate these characteristics. Conventional methods, such as the slump test and flow table test [32] are not sufficient to provide a distinct assessment of printability in 3DPC. Furthermore, the material undergoes continuous changes over time during the printing process [33], which underscores the necessity of developing reliable tools and frameworks for assessing and monitoring the fresh-state behavior of 3DPC. Extrudability of 3D printing materials is commonly evaluated through methods such as long-strip extrusion tests, plunger extrusion tests, extrusion index calculations, and extrusion rate experiments [33]. While these methods provide useful insights, they often rely on specialized equipment and indirect measurements of pressure, flow, or power consumption. In this study, a more practical and direct approach was developed to assess both extrudability and printability of concrete mixtures.

Several researchers have explored the use of various raw materials in 3D printed concrete (3DPC) to enhance its sustainability and fresh properties. Deng Q, Zou S, Xi Y et al. [17] have investigated the use of waste glass powder as partial cement replacement, where the results showed that up to 40 % replacement can reduce the drying shrinkage, improve durability and extend workability time, while procuring a greener product. For ready mix concrete, Ref [20] has used recycled aggregates and viscosity-modifying agents to improve the extrudability and buildability of 3D printed concrete by improving the secondary mixing rheological performance. On the other hand, other researchers such as [34] have extended their investigation beyond cementitious systems to examine 3D printing of lunar regolith simulants via vat polymerization, focusing on sintering conditions and mechanical strength for extraterrestrial construction. Although these studies highlight significant advances in 3DPC, the use of locally available UAE materials in developing the 3DPC mixtures and the detailed investigation of their fresh properties, rheology and printability make the current study distinct from the other available studies. Therefore, this study aids in addressing a critical research gap related to practical applications of additive manufacturing in the UAE construction.

The primary objectives of this study are: (1) to develop 3D printed concrete (3DPC) mixes utilizing locally available construction materials from industry; (2) to propose a practical on-site method for the rapid evaluation of 3DPC printability, addressing the industry's need for efficient and field-applicable assessment tools; and (3) to develop printability suitability charts that enable objective evaluation and quality control of 3D printed elements, thereby enhancing consistency and performance in real-world applications.

To achieve these objectives, a series of 3DPC mixes was formulated using UAE-sourced materials. The effects of fly ash and silica fume as supplementary cementitious materials, along with two types of synthetic fibers, were examined in relation to the fresh and rheological properties of the mixes. Additionally, the effect of water-to-binder (w/b) ratio on these properties was systematically investigated.

As part of the proposed quality control approach, a novel on-site evaluation method employing a manual mortar gun was introduced to assess the printability and buildability of 3DPC mixes. This method demonstrates potential for standardization and routine implementation in construction settings. Furthermore, printability suitability charts were developed to support the rational design and assessment of 3DPC mixes. Overall, the study offers practical insights and data-driven tools that can significantly aid the implementation and regulation of 3D concrete printing in the UAE, thereby contributing to the broader advancement of this emerging construction technology.

2. Experimental program

2.1. Materials

Type 1 Portland cement was used in this investigation to prepare and develop 3D printing concrete mixtures. Fly ash and silica fume were also incorporated into the 3D printed concrete mixtures. Table 1 shows the chemical and physical analysis for the used OPC, silica fume and fly ash.

A mid-range water-reducing admixture (superplasticizer) was incorporated into the mix. The aggregates are locally produced from a local crushing plant. The aggregates used had a maximum size of 4.75 mm. The absorption of the aggregates is 1 % and their specific gravity is 2.7. Fig. 1 shows the grain size distribution of the used aggregates and specification limits.

Two fibers were used in this investigation, namely HP 6 and stewathix 600 (ST600). The fiber HP 6 is a glass shortcut fiber with a circular cross section and an average fiber length of 6 mm. It has a specific gravity of 2.68 and is white/grayish. ST 600 is polyethylene fibroids with a kidney shape section and a 0.2–0.5 mm average length. Its specific gravity is 0.96 and its color is white. Fig. 2 shows the binder materials and fibers used in this investigation.

2.2. Experiments conducted

The selection of process parameters in this study was based on a combination of literature review, preliminary lab trials, and

Table 1
Chemical and physical analysis of used cementitious materials.

Description	Type 1 OPC %	Silica fume %	Fly ash %
SiO_2	19.85	88.70	52.02
Al_2O_3	4.79	0.58	25.03
Fe_2O_3	3.86	1.32	7.88
MgO	1.26	0.85	2.39
CaO	62.66	0.74	5.26
Na_2O	0.59	0.48	1.09
K_2O	–	1.37	1.62
MnO	–	0.081	0.08
TiO_2	–	0.008	1.15
Moisture content	–	0.61	0.12
LOI	3.37	4.69	1.60
Sulfate content (as SO_3)	2.70	–	–
Chloride content	0.07	–	–

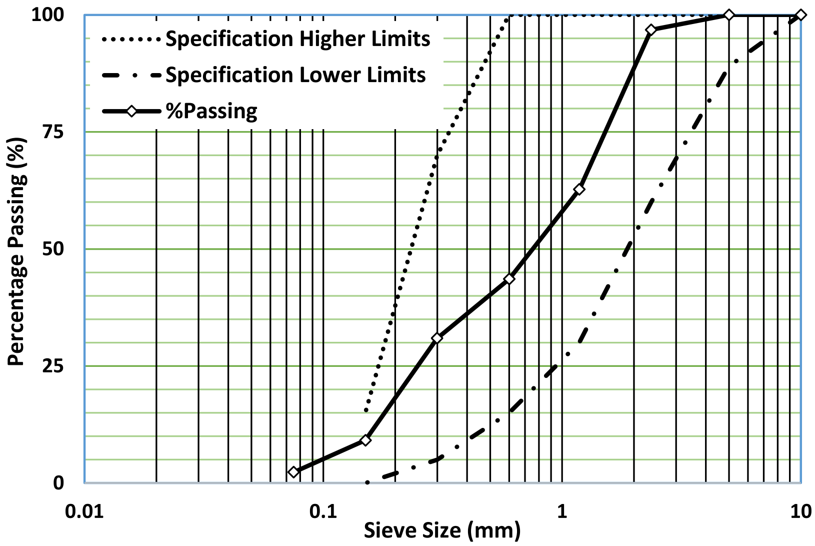

Fig. 1. Gradation curve of the used aggregates and specification limits.

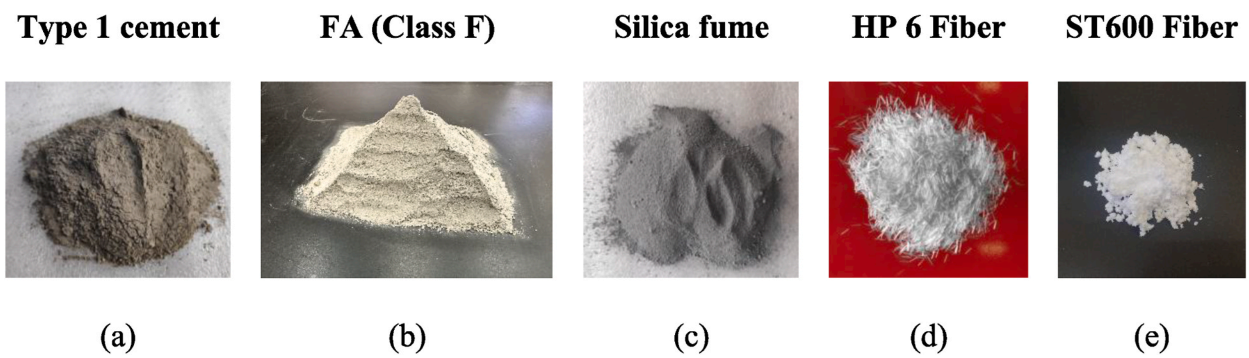

Fig. 2. Photos of the binder materials and fibers used: (a) Type 1 cement, (b) fly ash, (c) silica fume, (d) HP 6 fiber and (e) ST 600 fiber.

practical considerations related to 3D concrete printing applications [35]. The parameters investigated include water-to-binder ratio (w/b), fly ash (FA) content, silica fume (SF) content, fiber incorporation, and superplasticizer (SP) dosage. These variables are known to significantly influence the rheological behavior and fresh-state performance of 3D printable concrete, particularly in terms of extrudability, buildability, shape retention, and interlayer bonding [36].

The water-to-binder ratio was varied due to its fundamental role in controlling flowability, and dynamic yield stress, all of which directly impact printing quality during deposition. Fly ash and silica fume were selected as supplementary cementitious materials for their beneficial effects on workability and rheological properties, which are essential for ensuring good printability [37].

The inclusion of fibers was aimed at enhancing green-state stability and reducing cracking between printed layers, which is crucial for maintaining dimensional accuracy and structural performance [31]. The superplasticizer dosage was adjusted across mixes to

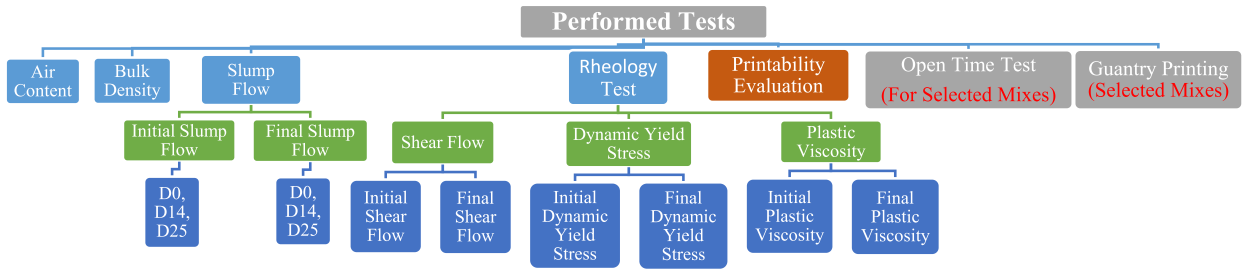

Fig. 3. Experiments conducted on studied 3D printed concrete mixes.

optimize flow without causing loss of shape retention.

While a formal statistical design of experiments was not applied, the parameter ranges and combinations were carefully chosen to reflect realistic field conditions and construction practices. This approach allows for a practical understanding of how individual material components affect the performance of 3D printed concrete, with direct relevance to scalable implementation in the construction industry.

The properties investigated in this research are shown in Fig. 3 and include the fresh mix properties, such as air content, bulk density, slump flow (initial and final), rheology including shear flow (initial and final), dynamic yield stress (initial and final) and plastic viscosity (initial and final) and printability evaluation. Additionally, for a set of selected mixes, the open time test was performed.

2.3. 3D concrete mix design

The 3D printing concrete mix design was performed following the absolute volume method (1 m^3). To carry out this investigation, three groups of mixes were studied (Table 2). The first mix group was proportioned to study the effect of the change in fly ash replacement dosage on the studied properties at specified w/b ratios and superplasticizer (SP) dosages. This mix group was divided into two subgroups (G11 and G12) with fly ash replacement levels of 0 %, 25 %, 30 %, 45 %, and 50 %. For subgroup G11 the w/b and superplasticizer dosage were taken to be 0.48 and 2 %, respectively, whereas for G12 the w/b and superplasticizer dosage were taken to be 0.53 and 1.5, respectively. The second group was divided into two subgroups (G21 and G22) with the fly ash replacement level taken as 36 %. Subgroup G21 was proportioned to study the effect of changing the w/b (0.46, 0.48, 0.5, 0.51, and 0.53) with a constant SP dosage of 2 %. On the other hand, subgroup G22 was proportioned to study the effect of SP dosage change of (1.15 %, 1.3 %, 1.5 %, 1.65 %, 1.8 % and 2 %) at a constant w/b of 0.53. The last group consists of three subgroups (G31, G32 and G33) with a fly ash (FA) replacement of 36 %, w/b of 0.53 and an SP of 2 % for the first two subgroups and an SP of 1.65 % for the third subgroup. This subgroup aims to investigate the effect of adding fiber and silica fume (SF) on the studied properties. In subgroup G31, Stewathix 600 (ST600) fiber was incorporated in the mixes with dosages of (0 %, 0.11 %, 0.15 %, 0.22 % and 0.25 %), whereas in subgroup G32 the glass short cut - FGCS HP (HP6) fiber was incorporated in the mixes with dosages of (0 %, 0.15 %, 0.22 % and 0.3 %). The third subgroup G33 had silica fume (SF) incorporated as a partial replacement to OPC with the following percentages (0 %, 5 % and 10 %). The fly ash percentage of 36 % was used in both G2 and G3 mixes as it reflects the recommended fly ash percentage by Dubai municipality and thereby it is widely used in the UAE concrete industry.

Table 2
Compositions of 3D printed concrete mixes studied in this research and their corresponding names.

Group	Subgroup	Name	W/b	SP %	Sand kg/m^3	Fly ash %	Silica fume %	ST600 fiber %	HP6 fiber %
G1	*G11*	*G11-FA0*	0.48	2	1760	0	0	0	0
		G11-FA25	0.48	2	1760	25	0	0	0
		G11-FA30	0.48	2	1760	30	0	0	0
		G11-FA45	0.48	2	1760	45	0	0	0
	G12	*G12-FA0*	0.53	1.5	1760	0	0	0	0
		G12-FA25	0.53	1.5	1760	25	0	0	0
		G12-FA30	0.53	1.5	1760	30	0	0	0
		G12-FA45	0.53	1.5	1760	45	0	0	0
		G12-FA50	0.53	1.5	1760	50	0	0	0
G2	G21	*G21-WC46*	0.46	2	1760	36	0	0	0
		G21-WC48	0.48	2	1760	36	0	0	0
		G21-WC50	0.50	2	1760	36	0	0	0
		G21-WC51	0.51	2	1760	36	0	0	0
		G21-WC53	0.53	2	1760	36	0	0	0
	G22	*G22-SP1.15*	0.53	1.15	1760	36	0	0	0
		G22-SP1.3	0.53	1.3	1760	36	0	0	0
		G22-SP1.5	0.53	1.5	1760	36	0	0	0
		G22-SP1.65	0.53	1.65	1760	36	0	0	0
		G22-SP1.8	0.53	1.8	1760	36	0	0	0
		G22-SP2	0.53	2	1760	36	0	0	0
G3	G31	*G31-ST0*	2	0.53	1760	36	0	0	0
		G31-ST0.11	2	0.53	1760	36	0	0.11	0
		G31-ST0.15	2	0.53	1760	36	0	0.15	0
		G31-ST0.22	2	0.53	1760	36	0	0.22	0
		G31-ST0.25	2	0.53	1760	36	0	0.25	0
	G32	*G32-HP0*	2	0.53	1760	36	0	0	0
		G32-HP0.15	2	0.53	1760	36	0	0	0.15
		G32-HP0.22	2	0.53	1760	36	0	0	0.22
		G32-HP0.3	2	0.53	1760	36	0	0	0.3
	G33	*G33-SF0*	1.65	0.53	1760	36	0	0	0
		G33-SF5	1.65	0.53	1760	36	5	0	0
		G33-SF10	1.65	0.53	1760	36	10	0	0

2.4. Concrete mixing

A pan mixer with 60 L capacity was used throughout this experimental program. The mixing of concrete constituents was performed consistently for all 3D printed concrete mixes. First, the aggregates were placed in the pan and dry mixed for 1 min. Then, the binder materials (cement and supplementary cementitious materials (SCMs)) and/or fibers were added, and the mixer ran for an additional 1 min. Afterward, water along with admixture was added gradually and the mixer was left to mix for 3 min until it was ensured that the mix was homogeneous. The mixer was stopped, and the following tests were performed: slump flow test, air content, rheology test and bulk density test. Then the materials were left undisturbed in the pan mixer under standstill conditions for 1 h, and the cover of the pan was closed to prevent water evaporation. The mixer was turned for 1 min and the slump flow test and rheology test were repeated. The results for the first set of tests are named herein as initial and the results after 1 h of mixing were denoted as final. Below brief descriptions of some main tests are presented. It should be noted that the procedure used involved prolonged mixing of concrete and conducting several experiments. The mixing procedure in this investigation was tailored considering both the ASTM C685-0217 guidelines and that reported by Ref. [38].

2.5. Testing equipment

2.5.1. Slump flow table

The slump flow test, which determines the quality of concrete concerning its consistency and cohesiveness, was measured using the slump flow table. The slump flow of concrete strongly affects the dynamic yield stress, which in turn influences its pumpability and extrudability. Fig. 4 shows the slump flow table and pertinent tools used in this study. The slump flow table testing was done in accordance with BS EN 12350-5 (Testing Fresh Concrete – Flow Table Test).

2.5.2. Rheometer

An advanced ICAR concrete rheometer was used in this investigation to measure the rheological properties of 3D printed concrete. The ICAR is a portable rheometer; it is suitable for performing onsite rheological evaluation for the 3D printed concrete mixes. The rheometer comprises a container, a driver head, vane geometry, and a holding frame for securing the fixed driver head (refer to Fig. 5). The inner container's circumference has vertical ribs spaced equally to prevent potential slippage of the tested concrete. The container has an inner diameter of 405 mm and a height of 460 mm. The driver's head is equipped with an electrical torque motor linked to a vane with four blades, the vane radius is 63.5 mm and it has a height of 127 mm (see Fig. 5). The vertical and horizontal gaps between the inner wall of the container and the vane's blades are four times the maximum aggregate size (40 mm). The application of torque to the tested concrete is executed through the rotation of the vane blades.

2.5.3. Manual printing equipment

The developed concrete mixtures were printed manually using a grout pump. Fig. 6a shows the grout pump used to print the tested 3D concrete mixtures. The cylinder of the pump has a diameter of 5.5 cm (Fig. 6b) and the dimensions of the opening of the nozzle are 4 cm by 1.6 cm (Fig. 6c). Printing was conducted carefully to ensure the consistent dimensions of the printed layers. After mixing, the

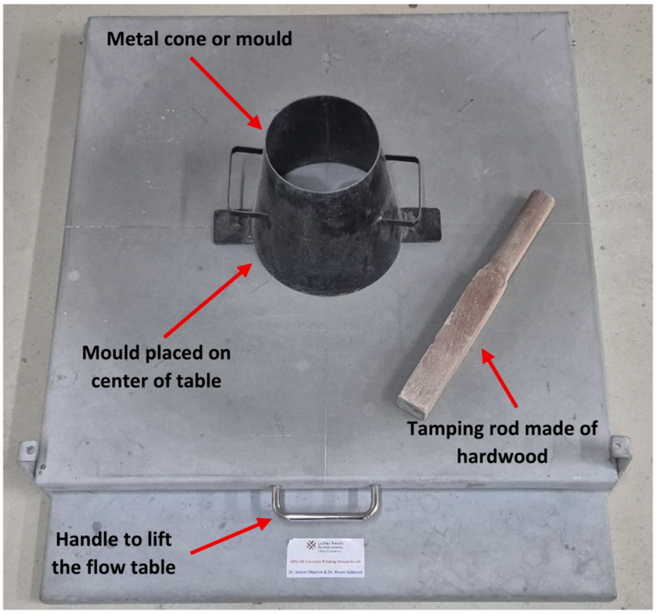

Fig. 4. Photo of the slump flow table and pertinent tools used in this study.

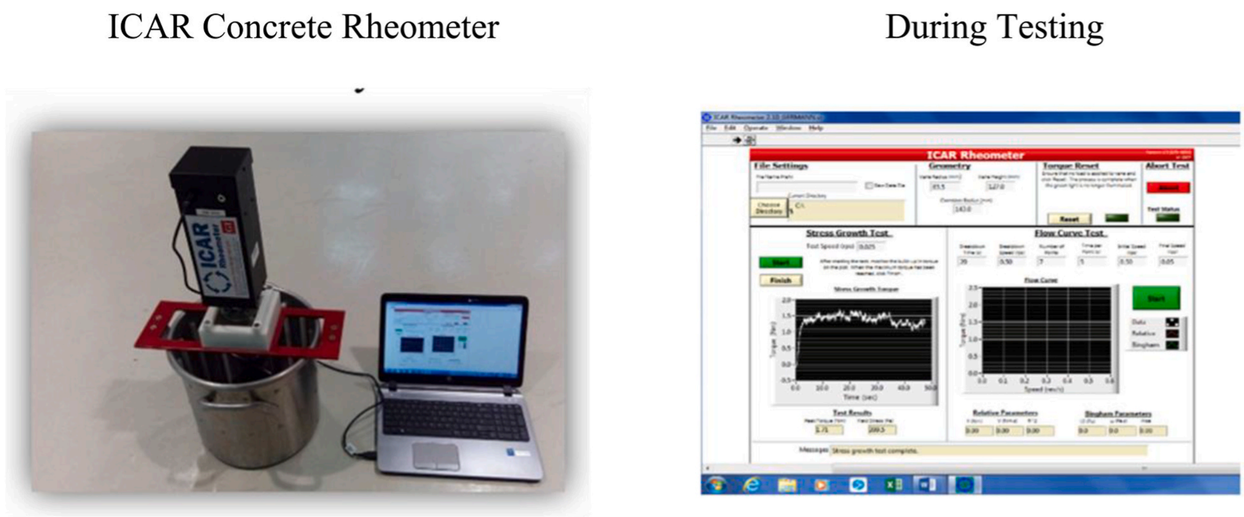

Fig. 5. ICAR concrete rheometer.

cylinder of the pump was filled with the concrete mix. The concrete was extruded from the nozzle manually by pressing on the piston. Then, the concrete was printed layer by layer. Fig. 6d shows 3D printing a 3D concrete filament using the manual pump. The target maximum number of layers for evaluating the buildability of 3D printed concrete mixes was five layers (Fig. 6e). The total height of the printed layers was measured to assess buildability. The extrudability (pumpability) of the developed 3D printed mixture was qualitatively evaluated by the force/effort that the research assistant required to push the piston to extrude the material inside.

2.6. Testing procedures

2.6.1. Slump flow testing

The surface of the flow table was cleaned of dust or other dirty materials. The concrete was placed into the mold in two layers, and

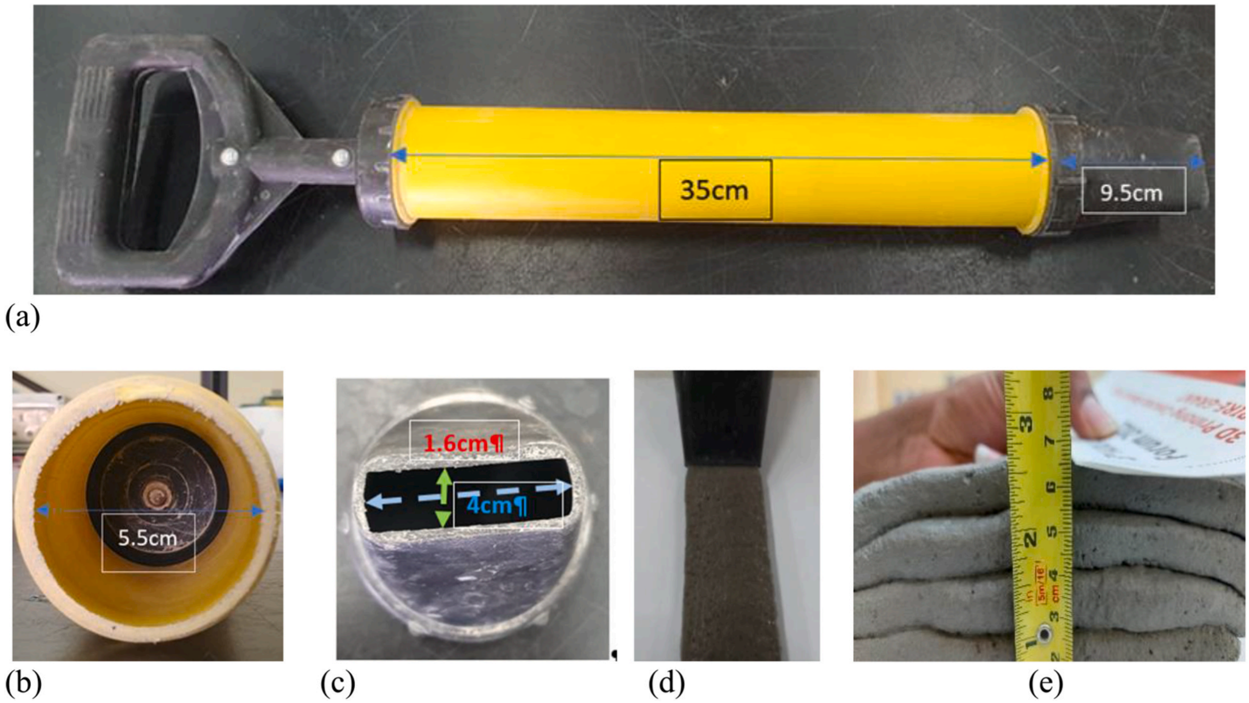

Fig. 6. The manual grout pump used: (a) the whole system, (b) the internal section of the nozzle (c) the rectangular opening of the nozzle, (d) printing a 3DPC layer and (e) 3D printed concrete sample (5 layers).

each layer was tamped 25 times using a tamping rod. The overflowed concrete on the last tamped layer was struck using a trowel. Then the cone was slowly lifted vertically and the concrete stood on its own weight without any support. Two perpendicular diameters of the spread concrete were measured, and their average was recorded as the value of the initial diameter (D_0). The flow table was raised to a height of 12.5 mm and dropped 15 times and then two perpendicular diameters were measured, and the average was calculated and recorded as the middle diameter (D_{15}). Lifting and dropping of the flow table were repeated for an additional 10 times and the average of two perpendicular diameters was recorded as the final diameter (D_{25}). These procedures were strictly followed for all tested 3D printing concrete mixes in this study. Fig. 7a–c presents the slump flow measurements (D_0, D_{15}, and D_{25}) of one of the studied mixes. The flow table test for all 3DPC mixes was conducted twice: initial time (immediately after concrete mixing) and final time (after 1 h) to evaluate the effect of time on the fresh properties of 3D printed concretes.

2.6.2. Rheology testing

The ICAR concrete rheometer was used to perform shear flow tests. The sequence of the shear flow is shown in Fig. 8. To create uniform conditions by breaking down the structure before testing, the concrete was first pre-sheared for 20 s at a shear rate of 0.5 rps. During the following 30 s, the rotational speed (shear rate, N, in revolutions per second [rev/s]) was decreased in a stepwise manner from 0.5 to 0.05 rps (Fig. 8). To reduce the potential segregation during testing, the down-curve was considered, because the time required to reach equilibrium at each shear rate is shorter than the up-curve [39]. The torque resistance of concrete T (N.m) at each of the different rotational speed increments was measured by the ICAR, and data points of torque vs rotational speed were employed to produce the flow curve. The results are fitted to a straight line using Eq. (1). The yield value G (N.m) is the intercept of the fitted straight line to the torque axis, and the viscosity factor H (N.m.s) is the slope of the line.

To obtain the dynamic yield stress (τ_o) and plastic viscosity (μ), the Reiner-Rivlin equation (Eq. (2)) is used:

$$T = G + HN \tag{1}$$

$$\Omega = \mathrm{T} / 4\pi \mathrm{h}\mu \left(1 / \mathrm{R}_i^2 - 1 / \mathrm{R}_o^2\right) - \tau_o / \mu \ln(\mathrm{R}_o / \mathrm{R}_i) \tag{2}$$

$$\Omega = 2\pi \mathrm{N}$$

where,

Ω is the angular velocity of the outer cylinder (rad/s);
h is the height of the inner cylinder (m);
R_i is the radius of the inner cylinder (m);
R_o is the radius of the outer cylinder (m).

It should be noted that the dynamic yield stress is the critical shear stress under which no flow occurs, or represents the onset of the flow from rest. Viscosity, on the other hand, is the resistance of a fluid to flow due to internal friction between its particles.

2.6.3. Manual printing and evaluation

Printability is defined as the ability of a mixture to extrude (extrudability) and maintain structural integrity when built in layers (buildability) [9]. In the course of this research, a rating procedure to qualitatively and quantitatively evaluate and rate the printability of 3D concrete mixes was developed as outlined in Table 3. The procedure relied on manually printing the evaluated mixes using the grout pump described earlier (see Fig. 6) with aiming to print a 15 cm long and 5 cm wide filament for a total of 5 layers on top of each other, and then applying the developed qualitative and quantitative evaluation parameters to assess the printability of the selected mix.

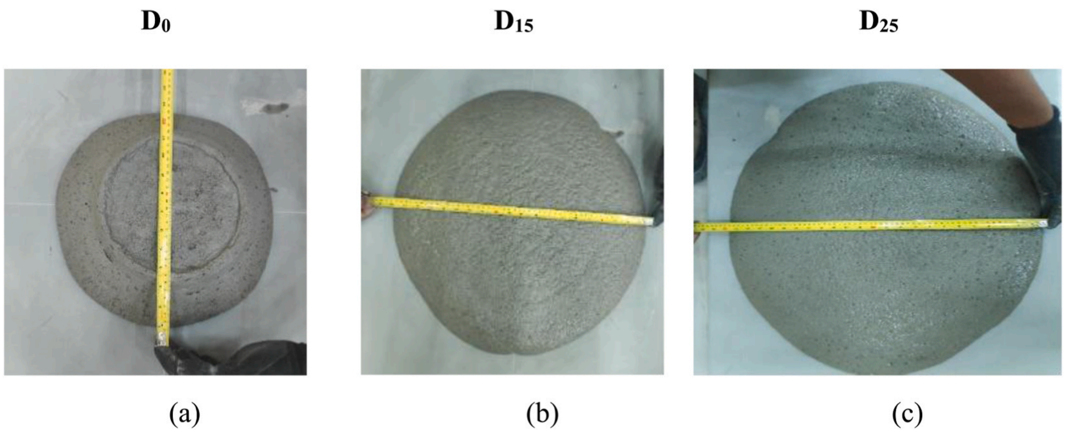

Fig. 7. 3D printed concrete sample tested: (a) apparatus, (b) the cone, (c) 0 blows measuring D0, d) 15 blows measuring D15, and (e) 25 blows measuring D25.

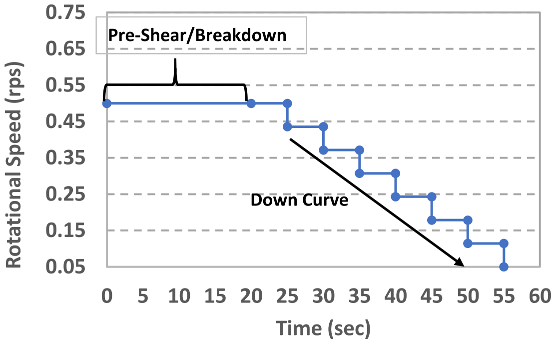

Fig. 8. Sequence of the rheology testing.

The qualitative evaluation consisted of observing the effort needed to extrude the mix and the level at which the layers collapsed after printing the 5-layer sample (if the mix prints). The extrusion of a mix is the movement of the pumping piston required to push the 3DPC to travel to and out of the nozzle. The force applied to the 3DPC depends on the developed stress between the material and the wall of the pump (i.e., the cylinder); it needs to be as low as possible to avoid blockage [8]. This implies that the dynamic yield stress should be as low as possible to ensure smooth and adequate pumpability of the 3DCP mixtures [40]. The printed samples were evaluated quantitatively by measuring the height of the 5 printed layers at three positions: middle, and both ends and then the average height was calculated to assess the buildability of the mixes. Based on both the qualitative and quantitative evaluation results, the 3D printed concrete mix was given a rating from 0 to 4, and a description was detailed in Table 3.

This proposed rating procedure can be used as a tool for quality control testing and initial evaluation of the suitability of the 3D printing concrete mixes. The procedure is a simple and fast test that can be performed onsite and takes less than 1 min and can, to a

Table 3
3D printed concrete mixes rating evaluation procedure.

Rate	Description	Qualitative Evaluation Criteria	Quantitative Evaluation Criteria	Sample
1	Fairly extrudable	– The mix is stiff and not easily extrudable – Needed to put excessive force to push the grout pump to extrude	– Less than 5 layers extruded	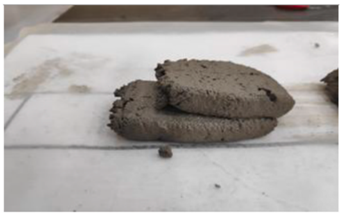
2	Extrudable and not buildable	– The mix is very soft and easily extrudable. – The mix can be printed in a 5 layer sample, but layers are collapsing.	– layers extruded – Average height of 5 layers less than 4 cm	
3	Extrudable and fairly buildable	– The mix is soft and easily extrudable – The mix can be printed in a 5 layer sample, but layers are slightly collapsing	– layers extruded – Average height of 5 layers between 4 cm and 6 cm	
4	Extrudable and buildable	– The mix was relatively soft and extrudable – The mix can be printed in a 5 layer sample, and layers are stable and not collapsing	– layers extruded – Average height of 5 layers 6 cm or more	

good extent, evaluate the printability and buildability of the 3D-printed concrete mixes. This onsite fast testing method was employed routinely by the current authors to evaluate the printed concrete mixes used to print large-scale elements and furniture such as twisted columns, fences and seats employing the large-scale gantry printer before printing. Some photos of these printed elements will be presented at the end of this paper.

3. Experimental results

During pumping, the 3D printed concrete should have adequate fresh and rheological properties [40]. It should be noted that fresh properties of concrete refer to the characteristics of concrete in its plastic state. This is vital to ensure that 3D printed concrete will not

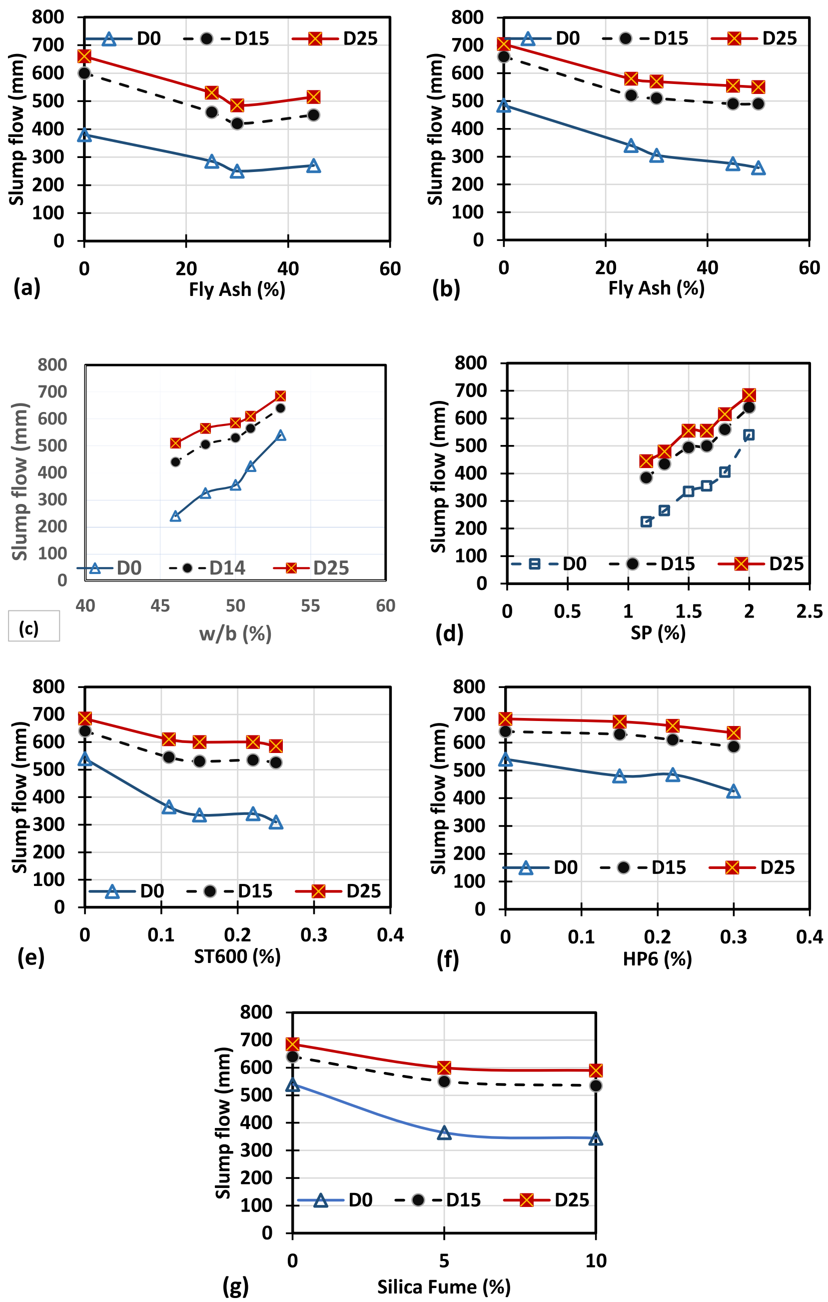

Fig. 9. Initial slump flow results: (a) G11 (w/b = 0.48, SP = 2 %), (b) G12 (w/b = 0.53, SP = 1.5 %), (c) G21 (FA = 36 %, SP = 2 %), (d) G22 (FA = 36 %, w/b = 0.53), (e) G31 (FA = 36 %, w/b = 0.53, SP = 2 %), (f) G32 (FA = 36 %, w/b = 0.53, SP = 2 %), (g) G33 (FA = 36 %, w/b = 0.53, SP = 1.65 %).

clog the pipe during pumping and will be placed smoothly to construct the desired printed object. Accordingly, the dynamic yield stress and viscosity should be adequate. During pumping, the bulk of the material in the pipe is not sheared; however, the shear is localized in a very narrow zone ([41–43]). The ability of a material to form a lubrication layer with the surface of the pumping pipe is essential for successful extrusion and printing. This lubrication layer is mainly water and fine particles. The ability to form such a lubricating layer change significantly with the water content of the mixture. As such, mixtures with low water content will have high dynamic yield stress and plastic viscosity, and they are not able to form this lubricating layer, which is essential for extrusion and printability. Such mixtures require extremely high pumpability pressure. The water to binder ratio (w/b) was selected for the 3DPC mixes in this study, considering what was discussed.

The following paragraphs present the fresh and rheological properties of the 3D concrete printed mixes studied in this research

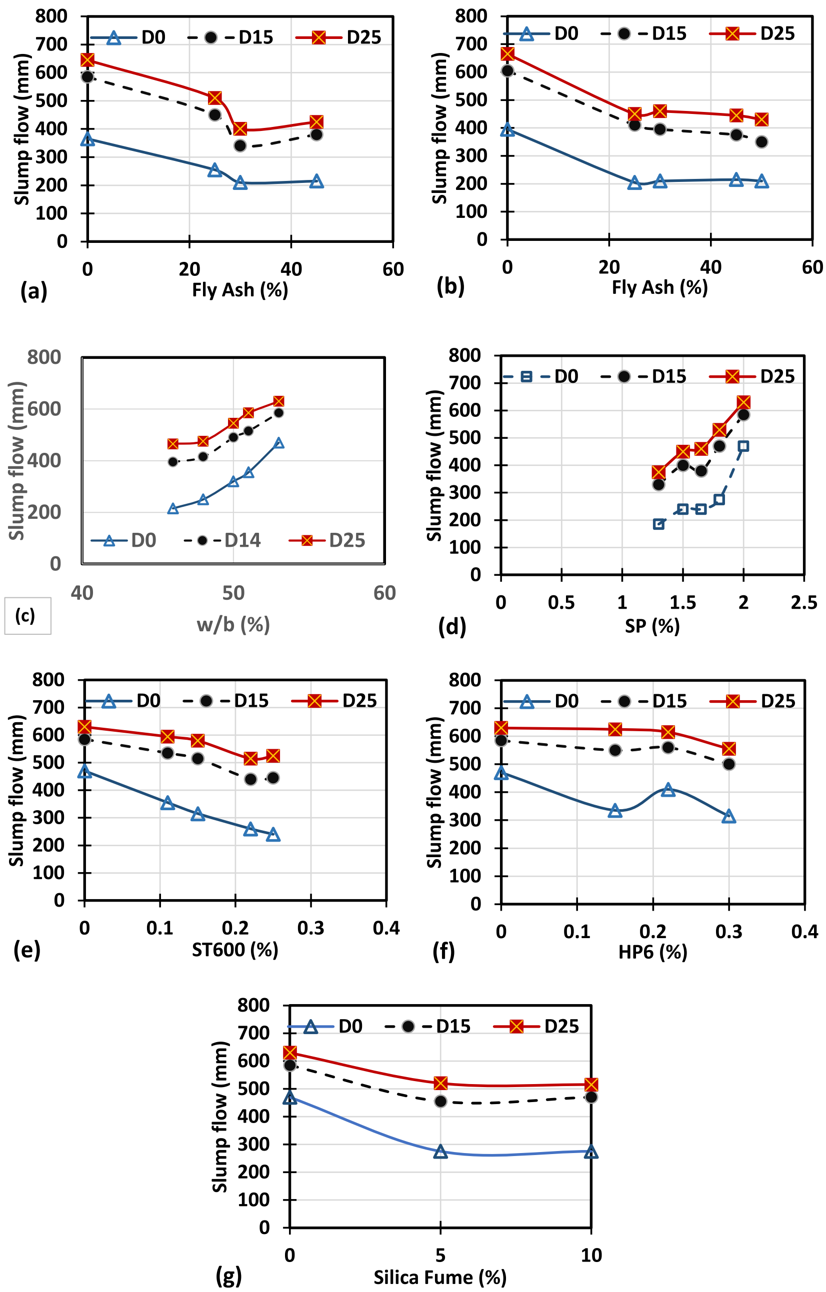

Fig. 10. Final slump flow results: (a) G11 (w/b = 0.48, SP = 2 %), (b) G12 (w/b = 0.53, SP = 1.5 %), (c) G21 (FA = 36 %, SP = 2 %), (d) G22 (FA = 36 %, w/b = 0.53), (e) G31 (FA = 36 %, w/b = 0.53, SP = 2 %), (f) G32 (FA = 36 %, w/b = 0.53, SP = 2 %), (g) G33 (FA = 36 %, w/b = 0.53, SP = 1.65 %).

program. The studied properties consisted of the slump flow (initial and final), shear flow (initial and final), dynamic yield stress (initial and final), and plastic viscosity (initial and final). The air content for all the studied mixes had an average value of 2.6 % with a standard deviation of 0.36. Whereas the average bulk density was 2235 kg/m^3 with a standard deviation of 14.5.

3.1. Slump flow

3.1.1. Initial slump flow

The initial slump flow curves for all studied 3DPC mixes are presented in Fig. 9. Three curves are included in each figure namely, D_0 (zero blow), D_{15} (15 blows), and D_{25} (25 blows). In general, the highest slump flow measurement is observed after 25 blows (D25), followed by those after 15 blows (D15) and 0 blows (D0). When analyzing the results of G1 mixes it is clear that FA has a negative effect on slump flow, where slump flow for 3DPC incorporating FA decreased with the increase in the FA dosage (Fig. 9a and b). This

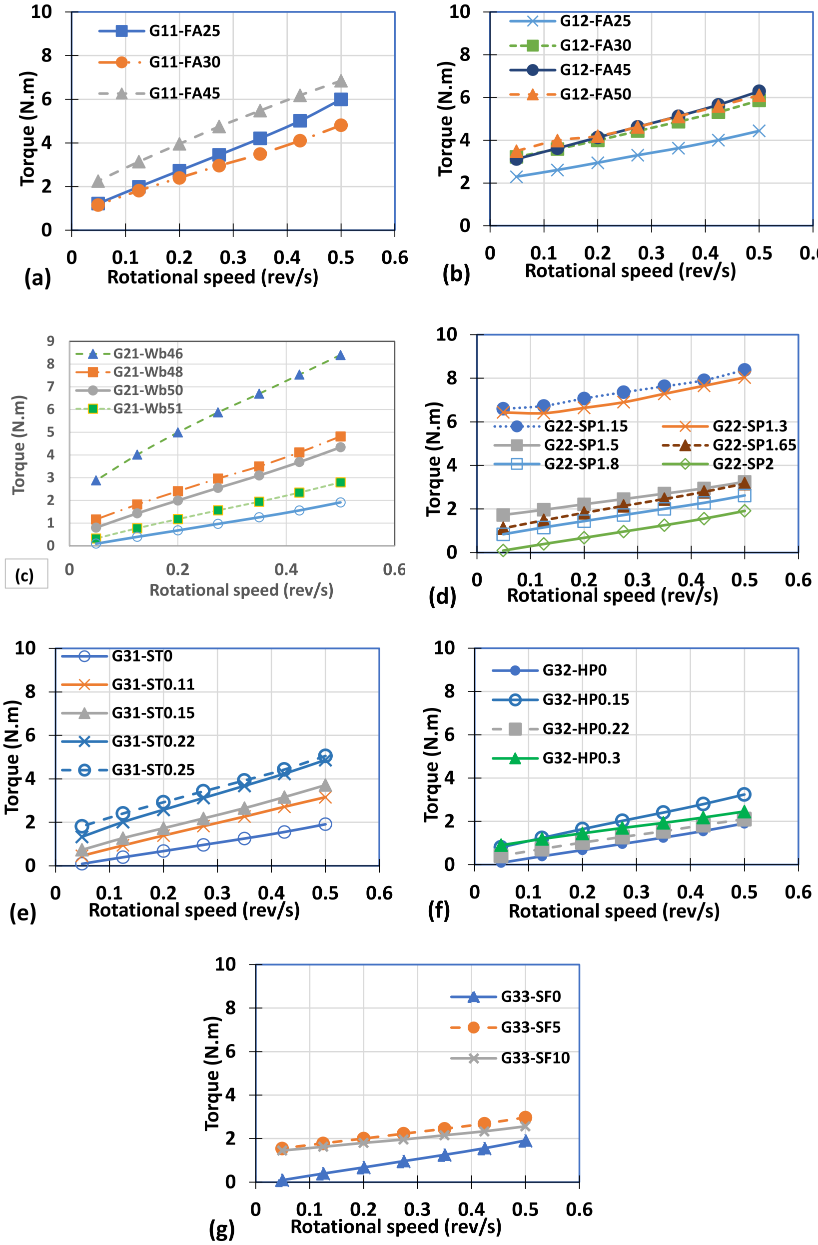

Fig. 11. Initial flow curves: (a) G11 (w/b = 0.48, SP = 2 %), (b) G12 (w/b = 0.53, SP = 1.5 %), (c) G21 (FA = 36 %, SP = 2 %), (d) G22 (FA = 36 %, w/b = 0.53), (e) G31 (FA = 36 %, w/b = 0.53, SP = 2 %), (f) G32 (FA = 36 %, w/b = 0.53, SP = 2 %), (g) G33 (FA = 36 %, w/b = 0.53, SP = 1.65 %).

observation applies to both subgroups G11 and G12. The results of the mixes in G21 and G22 show that the effects of both w/b and SP dosage on slump flow measurements are similar, where they increased with the increase of the w/b or SP dosage, as presented in Fig. 9c and d, respectively. For subgroups G31 and G32, results showed that the fibers have an inverse impact on slump flow. The slump flow decreased with the increase of fiber dosage for both types, as shown in (Fig. 9e and f). The results of G33 showed that the slump flow decreased with the increase in the SF dosage. However, the slump flow measurements showed less sensitivity to the change in SF dosages than for the change in FA dosages. (Fig. 9g).

3.1.2. Final slump flow

The final slump flow results for all studied 3DPC after 1 h are displayed in Fig. 10. Similar to the initial slump flow for G1 mixes that incorporated FA, the final slump flow decreased with the increase in the replacement dosage of FA. The patterns of the curves are very similar to the corresponding curves for the initial slump flow, with a slight decrease in the slump flow values indicating a good slump retention for all studied mixes. It can be depicted that the dosage of 25 % FA from G12 (SP = 2 % and w/b = 48 %) was the best in terms of slump retention among all G1 3DPC mixes studied. All measurements for initial and final mixing were comparable. The effects of w/b and SP dosage on the final slump flow are similar to those for the initial slump flow, where the measurements increased with the increase of these two factors. Like that of the initial slump flow, the final slump flow for 3DPC with fibers (G31 and G32) decreased with increased dosage of these two fibers (Fig. 10e and f). The curves related to G33 incorporating SF also indicated similar final slump patterns to those of the initial slump (Fig. 10g). The final slump values for mixes incorporating SF showed the most drop in the final slump compared to the initial slump indicating a lower slump retention.

3.2. Flow curves

In flow curve tests, the relationship between shear stress and shear rate is depicted. The yield stress is represented as the intercept of this curve with the shear stress axis, while the viscosity is indicated by the slope of the curve. In shear flow tests, the concrete microstructure is broken down and consequently, the measured yield stress will be significantly reduced. Hence, when the 3DPC (Three-Dimensional Printed Concrete) microstructure experiences stress beyond the yield stress, it breaks down, leading to a significant reduction in the measured shear stress. Although such tests can depict the rheological behavior of cement paste at continuous shear flow, i.e., during its pumping, and placing, they fail to define rheological properties at very low shear rates. For instance, viscous properties obtained from flow curves generally do not apply to a quiescent cement paste in a cast in place column [44]. Hence, the shear flow test can effectively capture the rheological behavior of 3DPC during continuous shear flow, such as during pumping and printing. However, they do not provide insights into the rheological properties of 3DPC before extrusion, or after printing a layer is completed i.e., at very low shear rates. Various empirical rheological models, e.g., Bingham, Herchel–Bulckley, modified Bingham, and Casson are used to estimate rheological parameters, i.e., yield stress and plastic viscosity, from experimental flow curves. The estimated cement paste rheological properties were found to vary when calculated using various models [44]. The Bingham model was adopted in this paper.

3.2.1. Initial flow curves

Fig. 11a shows the effects of fly ash on the initial flow curves for G11 3D printed concrete mixtures (w/b = 0.48 and SP = 2 %). The mix with 45 % FA had higher torque over the shear rate and mixes with 30 % FA and 25 % FA had comparable torque at a lower shear rate, but the 25 % FA had higher torque at a higher shear rate. It can be further observed that the mixes with 25 % FA and 35 % FA showed slight shear thickening, as the pattern of their flow curves was slightly concave upwards. A fluid with shear thickening behavior has a viscosity that tends to increase with a higher shear rate [45], due to the increase in the friction of flocculated particles [42,46]). The shear thickening is an exception case of what most complex fluids (like concrete) do when they are sheared, as they tend to organize themselves, reducing the friction between particles [45]. This is attributed to the shear-induced jamming transition [45]. Fig. 11b shows the effects of FA on G12 3D printed concrete mixes with high w/b (0.53) and low SP (1.5 %). Similar to the first set, the mixes showed slight shear thickening behavior, as the curves were slightly concaved upwards. However, the mix with 25 % FA had lower torque over the shear rate. The mixes with higher dosages of FA (50 %) required the highest torque at low rotational speed (up to 0.2 rev/s). This may be attributed to the high concentration of FA, resulting in FA particles colliding with each other at low shear rate and consequently requiring high torque. While fly ash typically improves workability due to its spherical shape, at high replacement levels (>30 %), it may increase torque at low shear rates, potentially due to enhanced particle interaction and binder dilution effects that alter the rheological response of the mix. It can be observed that FA promoted adhesion in 3DPC mixes, as generally a higher torque was required for a higher content of FA over the shear rate [47].

The effect of w/b ratio on the initial flow curve of G21 3DPC is presented in Fig. 11c. It can be noticed that when w/b is lower, 3D printed mixes require higher torque to print. It can be further depicted that the 3DPC displayed slight shear thinning behavior when w/b is low (0.46), as the flow curve is concaved downwards. This mix develops particle separation when subject to shear. When this mix was rated 1, according to the rating evaluation procedure introduced in this study, it was incapable of having continuous printed layers without tearing. However, the mix with w/b = 0.53 (high) was rated 3. It displayed clear shear thickening, and the flow curve was concave upwards. For G22 mixes, the shear thickening can be observed for 3D mixes with low superplasticizer dosage (1.15 %, 1.3 %), where the flow curves were concaved upwards. Although these two 3DPC mixes possess shear thickening behavior, they perform differently when printing. While the mix with SP = 1.15 was rated 1, the mix with SP = 1.3 % was rated 4. The higher the dosage of SP, the lower the required torque (Fig. 12d). The study of the G31 mixes showed that the effects of ST600 fiber are clear on the rheological behavior, as the shear thickening behavior can be observed on the initial flow curves for 3DPC mixes with ST600. Further, the higher the dosage of this fiber, the more required torque. Similar to G31 mixes with ST600 fiber, the higher the HP6 fiber (in G32 mixes), the more required torque. The introduction of SF resulted in a slight increase in the torque over the rotational speed for the studied mixes in G33. This is an indication of the adhesiveness and pozzolanic characteristics that SF possesses.

3.2.2. Final flow curves

The rheological behavior of 3DPC for all studied groups after 1 h was examined in Fig. 12. Clear shear thickening was observed for all 3DPC G11 mixes with high w/b = 0.53 and low SP = 1.5 and incorporating FA, as all shear flow curves were concaved upwards. Further, the higher the dosage of FA, the higher the torque over the rotational speed (Fig. 12a). The thickening behavior was not clear for 3DPC G12 mixes incorporating FA with a high dosage of SP of 2 % and low w/b of 0.48 (Fig. 12b). for these mixes the mix with 25 % FA had the lowest torque and the one with 45 % FA had the highest torque over the rotational speed (Fig. 12b). The effect of w/b on the

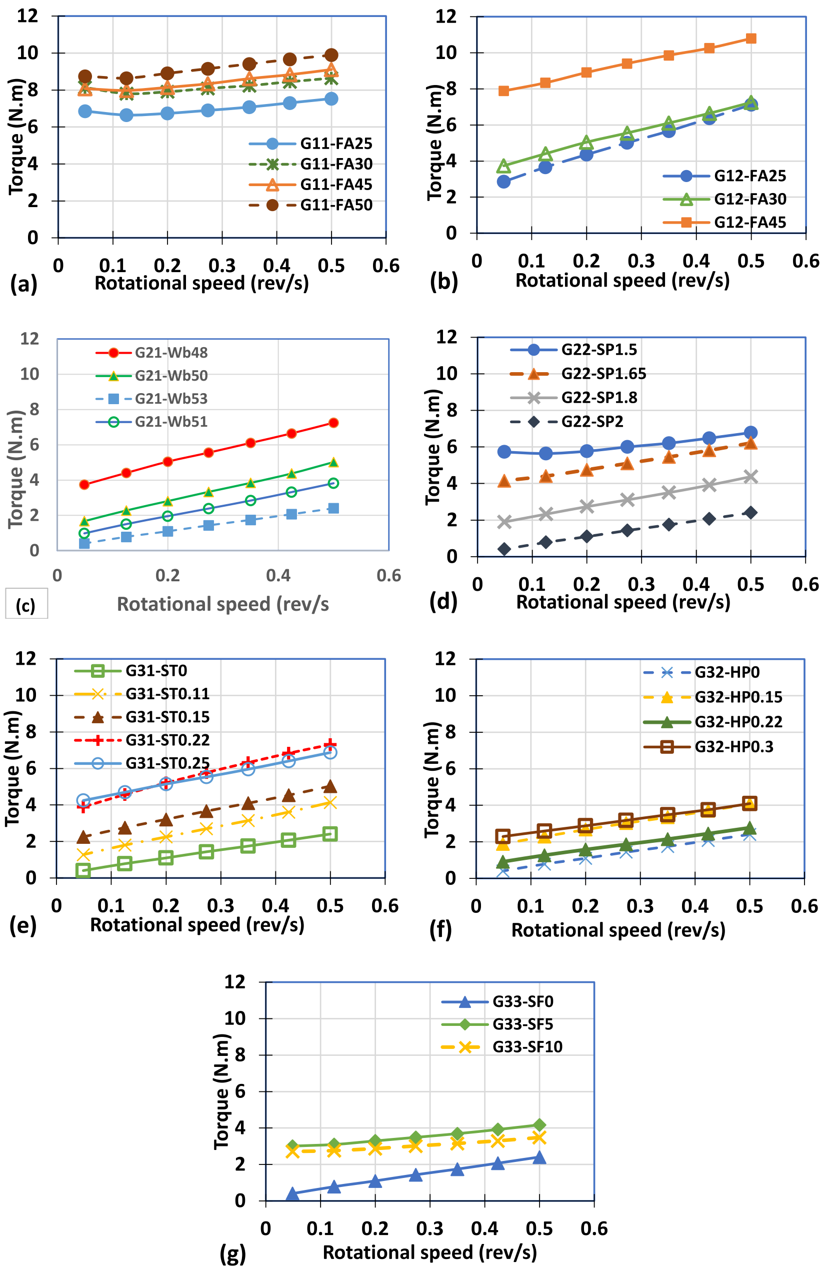

Fig. 12. Final flow curves: (a) G11 (w/b = 0.48, SP = 2 %), (b) G12 (w/b = 0.53, SP = 1.5 %), (c) G21 (FA = 36 %, SP = 2 %), (d) G22 (FA = 36 %, w/b = 0.53), (e) G31 (FA = 36 %, w/b = 0.53, SP = 2 %), (f) G32 (FA = 36 %, w/b = 0.53, SP = 2 %), (g) G33 (FA = 36 %, w/b = 0.53, SP = 1.65 %).

rheology of 3DPC G21 mixes after 1 h was displayed in Fig. 12c and it did not show clear shear thickening, but again the higher the w/b, the lower the torque. Fig. 12d shows the effect of SP dosage on the shear flow curves of 3DCP G22 mixes after 1 h. It should be noted that mixes with 1.15 % SP and 1.3 % SP are not included in the figure, as these mixes became stiff after 1 h and their rheology was not measured to avoid damaging the rheometer. The 3DPC at a high dosage of SP (1.5 %) showed clear shear thickening, whereas the rest did not. Again, the higher the dosage of the SP, the lower the torque over rotational speed (Fig. 12d). Fig. 12e shows the effect of ST600 fiber on the rheology of 3DPC G31 mixes after 1 h. No shear thickening behavior can be observed for the mixes in this mix group (Fig. 12e). The higher the dosage of ST600 fiber, the greater the torque. The 3DPC G32 mixes incorporating HP 6 fiber showed slight shear thinning at a low dosage of 0.22 %, as the shear flow curve was slightly concaved downwards. The 3DPC with a higher dosage had higher torque (Fig. 12f). Unlike FA, silica fume caused an increase in the torque and that is evidenced in the flow curves for G33 mixes incorporating SF, which showed shear thickening as these curves are concaved upwards.

The observed shear thickening behavior (Dilatant) for 3D printed concrete mixes indicates that when the shear rate is higher, the apparent viscosity is higher [45]. This is beneficial for promoting the cohesion between particles, due to the increase of particle

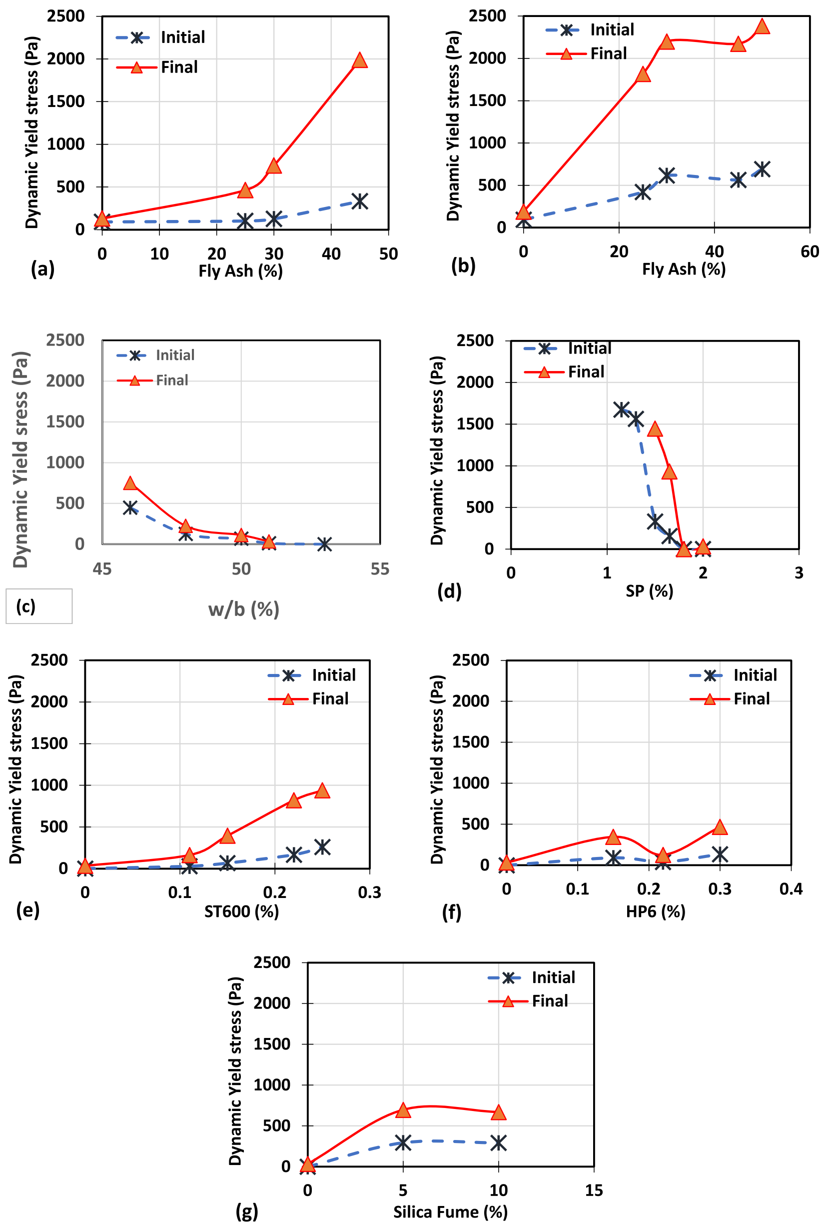

Fig. 13. Dynamic yield stress results: (a) G11 (w/b = 0.48, SP = 2 %), (b) G12 (w/b = 0.53, SP = 1.5 %), (c) G21 (FA = 36 %, SP = 2 %), (d) G22 (FA = 36 %, w/b = 0.53), (e) G31 (FA = 36 %, w/b = 0.53, SP = 2 %), (f) G32 (FA = 36 %, w/b = 0.53, SP = 2 %), (g) G33 (FA = 36 %, w/b = 0.53, SP = 1.65 %).

interactions when sheared. Concrete contains particles with anisotropic shapes and different sizes, and it is time dependent. When the concentration of particles in concrete is high (due for example, to low w/b or SP). The application of shear causes the rearrangement of solids, resulting in a mechanical jam. When exposed to shear forces, particles that are not spherical undergo precession. This will increase the volume that these particles occupy and consequently increase the effective concentration. Particles with larger sizes have higher inertia, which will cause them to retard for some time when they are sheared before they accelerate. Fluids with shear thickening, their particles agglomerate at a higher shear rate, resulting in more resistance. Therefore, a 3D printed concrete with shear thickening behavior, its particles will have enough time to reorder when subjected to a low shear rate. But if the shear rate is high, the particles will not have enough time to reorganize, and a significant shear force is built up. This is reflected in the shear flow curve. At low shear rate, torque decreases with an increase in shear rate, but beyond a certain shear rate, the curve increases with an increase in shear rate (increase in torque with shear rate). This may be attributed to the fact that the particles become agglomerated at the high shear rate and concrete requires higher torque, resulting in the shear flow curve being concave upwards. The printed mix with a higher shear thickening will exhibit more difficulty in printing [48].

On the other hand, fluid with shear thinning requires more torque when the shear rate increases. But when reaching a certain shear rate, (threshold value) a breakdown of its microstructure takes place leading to a decrease in the apparent viscosity at a higher shear rate. This will lead to a flow curve that will be concave downwards.

3.3. Dynamic yield stress

The yield stress is the shear stress required to initiate flow [49]. The yield stress is dependent on particle contacts. When strain in cement paste is very low, the cement particles stay in close contact with each other, and cement paste behaves in an elastic mode; it is able to recover elastically once the load is removed [50]. By increasing the shear stress, the strain will increase and the distance between particles will increase gradually until reaching a certain stress; particles are separated from each other, then the concrete starts to flow. This stress is called critical stress or yield stress [51].

The yield stress of concrete increases with time at rest, as it exhibits a thixotropic behavior. This is the case of the concrete in the formworks once it is cast, but this is not the case for the top layer of concrete, where fresh concrete is still flowing [49]. It is important to note that the rheological properties of concrete are also strongly shear history dependent [38]. The evolution of yield stress with time provides useful indications on the window of printability [52]. The upper limit of the printability window corresponds to the final time beyond which a 3DPC mixture becomes unprintable and cannot be extruded from the nozzle and the corresponding yield stress is designated as the upper bound, whereas the lower bound is the minimum yield stress required to keep the extrudate stable [53]. One of the key determinants of the printability of binder mixtures (including extrudability) is the dynamic yield stress of the fresh 3D printed concrete. The dynamic yield stress is a major factor in successfully printing concrete without the need for lateral formwork [2]. Thus, dynamic yield stress is an essential performance criterion to ensure adequate printability of 3D printed concrete mixtures (3DPC). To ensure the proper printing process of the 3DPC, the dynamic yield stress of 3DPC should not be high [54]. It was reported elsewhere [55] that the required shear strength for a 3D printed mixture to pass printability should be between 300 and 900 Pa. On the other hand, the static yield stress should be high enough to provide adequate layer stability to be able to carry its own weight and the layers above it [56]. Therefore, the 3DPC should be designed to have a suitable dynamic yield stress that meets the extrusion required to pass from the nozzle of the printing equipment and have an adequate static yield stress to build successive layers above each other with no lateral formwork.

Fig. 13 shows that the dynamic yield stress for the final mixing time (1 h) was higher than the initial mixing time. The dynamic yield stress of 3DPC G11 mixes incorporating FA with 2 % SP and w/b = 0.48 %, decreased slightly with a higher dosage for the initial mix, but it increased beyond a dosage of 26 % (Fig. 13a.). This suggests that for low w/b, the low dosage FA (26 %) can slightly promote the extrudability of 3DPC mixes at initial time. After on hour, dynamic yield stress increased progressively with higher dosage of FA, but the increase became steeper after a dosage of 26 % (Fig. 13a).

For 3DPC G12 mixes incorporating FA with low SP (1.5 %) and high w/b (53 %), the dynamic yield stress remained at a low level at the beginning of the hydration (initial), but increased slightly with a higher dosage of FA. But after 1 h of hydration, it increased sharply until a dosage of 36 % FA, then the increase was very marginal (Fig. 13b). This indicates that FA for G12 mixes with high w/b and low SP dosage requires extra force to be extruded. This was observed during the manual printing of these mixes after 1 h. The growth in dynamic yield stress with FA dosage is larger for final mixing than for initial mixing time.

Fig. 13c shows the effect of w/b on dynamic yield stress for 3DPC G21 mixes with 36 % FA and a dosage of SP = 2 %. The w/b ratio seems to promote the extrudability of 3DPC mixes as dynamic yield stress progressively decreased with higher w/b for initial and final hydration time (Fig. 13c). However, the gap between the final and initial curves decreased with increased w/b ratio and became marginal after w/b beyond 48 %. The curves for initial and final mixing times were very close. The effect of SP dosage is displayed in Fig. 13d. The dynamic yield stress for 3DPC G22 mixes decreased with higher dosages of SP. Data points for low dosages of SP after 1 h were missing, because the 3DPC mixes were stiff, and the rheology of those mixes was not measured to avoid damaging the instrument. This indicates that the SP at low dosage was effective temporarily, but when time elapsed, the repulsion and hindrance effect would be gone. Due to the attractive interparticle forces, the system will be more flocculated [57]. Hence, there will be more build-up on the interparticle forces, and the mix will be stiffer and with low workability.

Fig. 13e and f shows the effects of the fibers ST 600 (G31 mixes) and HP6 fibers (G32 mixes) on the dynamic yield stress. The w/b for these mixes was 53 %, the FA dosage was 36 % and the dosage of the superplasticizer was 1.65 %. As expected, the final mixing time curve was higher than the initial mixing time curve. The evolution in dynamic yield stress for ST600 3DPC G31 mixes was initially marginal, but it was significant after 1 h when the dosage of ST600 exceeded 0.1 %. This fiber should be used carefully in the case of prolonged printing, where it caused a progressed increase in the dynamic yield stress beyond a dosage of 0.1 %, which may increase the extrusion difficulty of the mix (Fig. 13e). The effect of HP6 fiber slightly promoted the dynamic yield stress, where the yield stress at final mixing time was slightly higher than initial mixing (Fig. 13f).

The addition of silica fume in G33 mixes increased the dynamic yield stress slightly, for both initial and 1 h hydration, but mixes with SF were extrudable. The dynamic yield stress for mixes with 10 % SF increased from almost 0 Pa for 0 % SF to 300 Pa and 700 Pa, for initial and 1 h, respectively. It was reported elsewhere [58] that the printability of 3DPC improved by adding silica fume, which helped in modifying the rheological properties and increasing the yield stress. The high specific surface area of silica fume may be why the dynamic yield stress increased with a higher dosage of SF, as its particles fill the gaps between the relatively large cement grains, thus causing interparticle friction due to increased interparticle contacts at a high dosage [37].

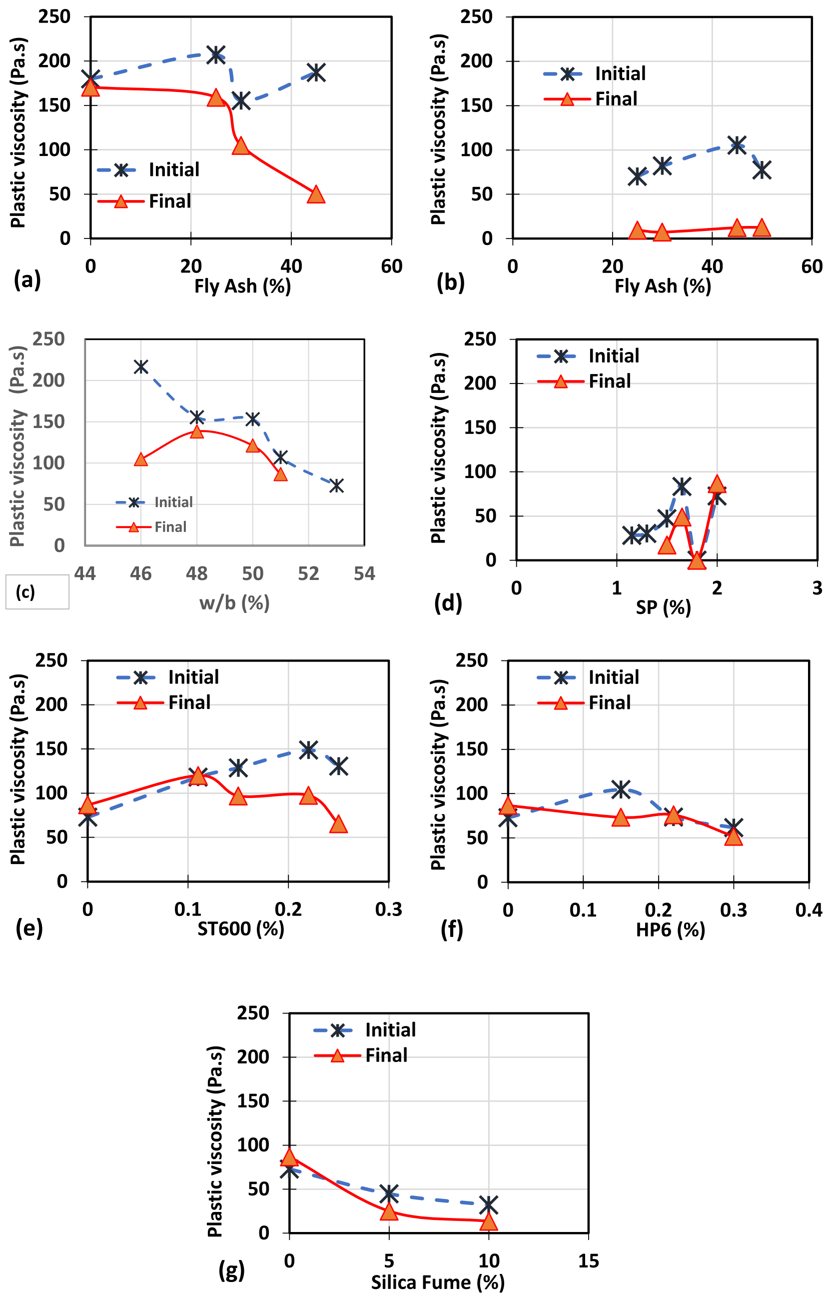

Fig. 14. Plastic viscosity results: (a) G11 (w/b = 0.48, SP = 2 %), (b) G12 (w/b = 0.53, SP = 1.5 %), (c) G21 (FA = 36 %, SP = 2 %), (d) G22 (FA = 36 %, w/b = 0.53), (e) G31 (FA = 36 %, w/b = 0.53, SP = 2 %), (f) G32 (FA = 36 %, w/b = 0.53, SP = 2 %), (g) G33 (FA = 36 %, w/b = 0.53, SP = 1.65 %).

3.4. Plastic viscosity

The measured plastic viscosity is the slope of the flow curve that was fitted to the Bingham model. It can be noticed from Fig. 14, that the evolution of viscosity at 1 h hydration was higher than the viscosity of the same mixes at initial hydration. The introduction of FA seems to have different effects on viscosity, depending on w/b and SP dosage. At w/b = 48 % and SP = 2 %, the incorporation of FA after a dosage of 26 % decreased the initial viscosity of 3DPC G11 mixes, while no clear change of plastic viscosity at 1 h hydration was observed (Fig. 14a). For G12 mixes with SP = 1.5 % and w/b = 53 %, the plastic viscosity was relatively low and did not show evident change with the dosage of FA. But after 1 h of hydration, the plastic viscosity increased slightly until 45 % FA and then it dropped (Fig. 14b). As expected, the initial and final plastic viscosities of 3DPC G21 with various w/b, decreased with increased w/b (Fig. 14c). No clear trend can be detected from Fig. 14d, for 3DPC G22 mixes with various SP dosages. The effect of ST600 fiber in G31 mixes is shown in Fig. 14e, where plastic viscosity increased with the fiber dosage until a certain dosage after which it decreased. No clear trend can be observed for the plastic viscosity of 3DPC G32 at various dosages of HP6 (Fig. 14f). The silica fume has a different effect on plastic viscosity compared to dynamic yield stress, the plastic viscosity for G33 mixes incorporating SF decreased with a higher dosage of SF (Fig. 14g).

4. Discussion

4.1. Relationships

Fig. 15 shows an inverse curvilinear correlation between dynamic yield stress and slump flow, with the data points having polynomial trend lines. Previous studies documented relationships between slump and yield stress. For example, Ref [39] reported exponential relationships between a slump and dynamic yield stress. Previously published studies by the current authors documented exponential correlations between yield stress and slump of SCC [50] and an inverse logarithmic correlation with a slump for flowable concrete under high temperature [38]. The correlation between slump and yield torque is recognized to be a negative curvilinear relationship with an exponential fit [59]. The importance of the correlations shown in Fig. 15 lays in the fact that the relationship between slump flow and dynamic yield stress is less documented in the literature, especially for 3DPC mixes.

No clear relationship between plastic viscosity and slump flow was depicted in Fig. 16, as the data points were scattered. This indicates that slump flow cannot be used to evaluate the plastic viscosity of fresh 3D printing concrete. The reason behind the weak correlation between plastic viscosity and slump flow is due to the fact that viscosity describes the flow behavior of concrete under flowing conditions, while slump flow is the flow behavior of concrete under standstill conditions. The stress required to overcome the interparticle forces and initiate flow is the yield stress and viscosity controls the behavior of a flowing fluid [60]. No relationship between slump and plastic viscosity was observed by Ref. [61]; they reported that slump is mainly related to yield stress. Further, no correlation between plastic viscosity and slump was reported by Ref. [50]. This suggests that the difference in the behavior of two concrete mixes having the same slump may be attributed to their differences in their viscosity values.

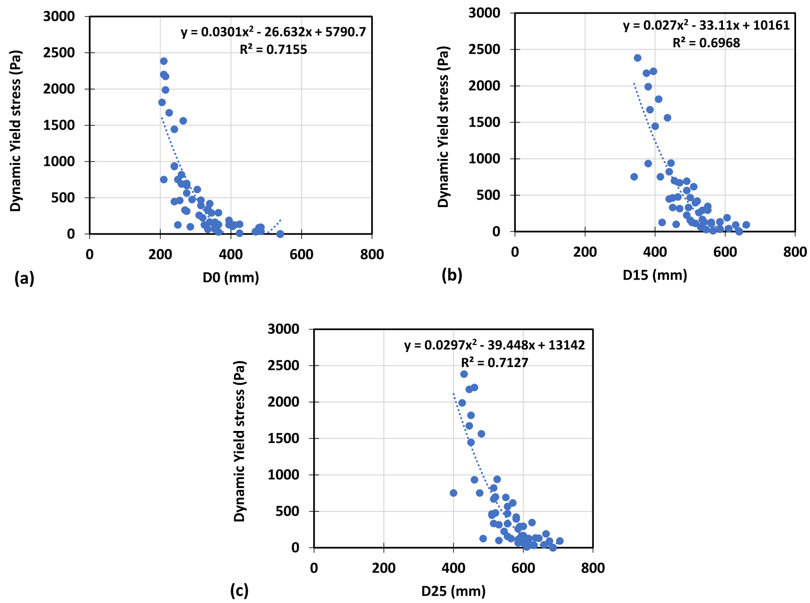

Fig. 15. Relationships between dynamic yield stress and: (a) D0, (b) D15, and (c) D25.

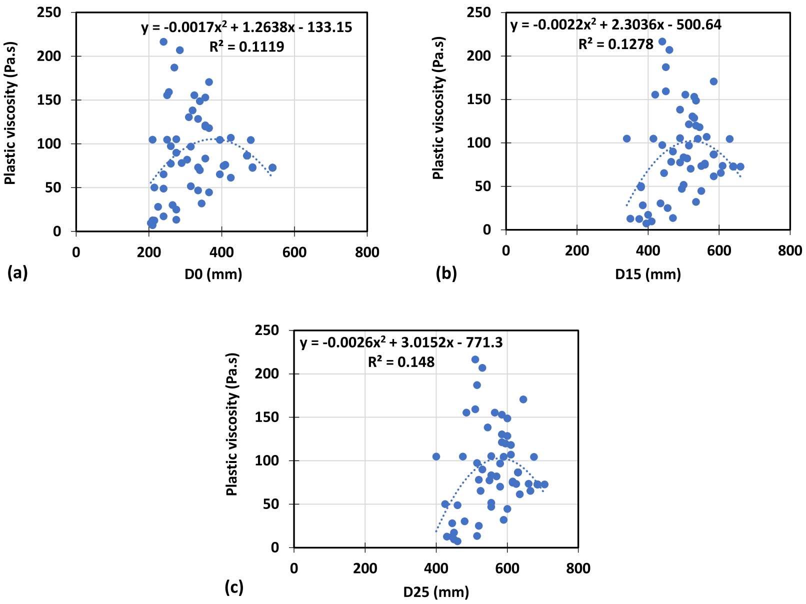

Fig. 16. Relationships between plastic viscosity and: (a) D0, (b) D15 and (c) D25.

4.2. Printability box

The structural element with 3D printed concrete is constructed through the buildup of relatively thin layers above each other. The layer's thickness ranges between 1 cm and 4 cm, which is thin when compared with the entire height of a wall (about 300 cm). To ensure this process is performed successfully, the layer should be flowable enough to be extruded but still gain sufficient strength in a relatively short time after extrusion to be able to carry the successive layers. To achieve the above goals, the paper attempted to propose a printability box to aid in identifying mixes that can satisfy the printability requirements. Accordingly, the dynamic yield stress was plotted versus the corresponding plastic viscosity for all studied mixes and for both initial and final results to construct a printability box that can aid in developing extrudable 3DPC mixes incorporating various SCMs and Fibers. This printability box can also assist in quality control and offer a valuable tool for objectively assessing the rheological properties of 3DP concrete mixes. Consequently, they play a crucial role in minimizing errors associated with the evaluation of fresh properties of 3DP concrete mixes. In traditional practices, simple field tests based on field experience and visual inspection, like the slump test, are often used to judge the flow behavior of concrete.

The extrudability and buildability of each of the studied mixes were evaluated once at the initial time (directly after mixing) and then again at the final time (after 1 h). Similarly, the dynamic yield stress and the plastic viscosity were measured at the initial and final times as discussed earlier in the results. For each of these cases (initial and final), the extrudability and buildability were rated based on the four different rating categories (Rate 1 to Rate 4) identified in the proposed rating system introduced earlier in this paper and described in Table 3. The printability charts created in this study were constructed by plotting both the initial and final dynamic yield stress against its corresponding initial and final plastic viscosity for each of the studied 3DPC mixes (Fig. 17) after labeling them based on their rating (each rating category was plotted with a distinguished symbol).

This printability chart showed that the mixes that rated 1 category had either low viscosity and high yield stress or high viscosity and relatively low yield stress. These mixes exhibited difficulty when being extruded (a maximum of two layers were only extruded). Fig. 17a and b shows that when the yield stress is relatively high, the plastic viscosity tends to decrease. This may be attributed to the fact that the slopes of the torque rotational speed curves for stiff mixtures are reduced. This observation is consistent with published research, which noted that plastic viscosity decreases over time for stiff mixtures, even if there is an increase in yield stress [39]. On this printability chart, a printability box containing only the 3DPC mixes that were rated 4 (extrudable and buildable) was located. This printability box showed that mixes having plastic viscosity values ranging between 15 Pa s and 97 Pa s, and the dynamic yield stress values ranging between 400 Pa and 1500 are expected to behave as Rate 4 category. Whereas most of the mixes allocated outside the printability box exhibited a rate from 1 to 3, which showed either no extrudability or fair to no buildability. This printability chart and the allocated box can aid in the mix design and quality control for 3DPC mixes and can reduce the amount of trial and error that is needed to reach a proper printable mix design. The results revealed that a medium dosage of ST600 fibers (0.11 %–0.22 %) and HP6 fibers (0.15 %–0.22 %) enhanced the extrudability and buildability of the 3DPC mixes, while simultaneously reducing the percentage flowability. These fiber-reinforced mixes were positioned within the defined printability box, indicating optimal fresh-state performance.

A low water-to-binder (w/b) ratio was found to be essential for achieving a satisfactory printable mix in the short term, placing the mixes within the printability box. However, to maintain printability over a longer duration, a higher w/b ratio is recommended to

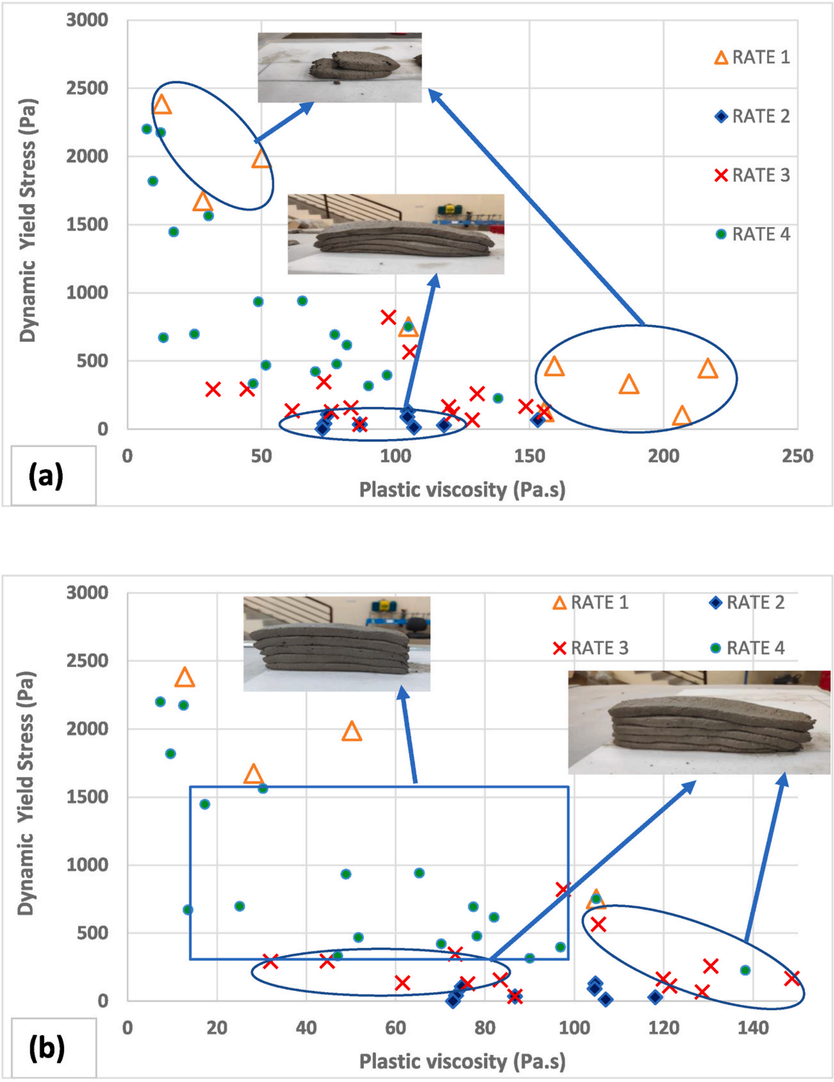

Fig. 17. Dynamic yield stress versus plastic viscosity (a) All data, (b) smaller range around the printability box.

counteract loss of workability due to thixotropic behavior and time-dependent stiffening.

In addition, the use of silica fume (SF) proved beneficial for short-term printability. Mixes containing MS were located within the printability box shortly after mixing, but fell outside the box after 1 h, indicating that their printability decreases over time.

4.3. Open time

Four mixes were selected to conduct the open time test, and the results are shown in Fig. 18. The picked mixes were initially rated 3 and finally rated 4 (after 1 h), as well as located in the printability box and were selected, such to represent different studied groups. The selected mixes are: G11-FA30 (30 % FA, w/b = 0.48, SP = 2 %), G33-SF10 (36 % FA + 10 % SF, w/b = 0.53, SP = 1.65 %), G32-HP0.3 (36 % FA, w/b = 0.53, HP6 = 0.30 %, SP = 2.0 %), and G31-ST0.25 (36 % FA, w/b = 0.53, ST600 = 0.25 %, SP = 2.0 %). The G11-FA30 mix had an initial dynamic yield stress of 126 Pa and a final dynamic yield stress of 752 Pa, it was rated initially 3 and finally 4. The G33-SF10 mix had an initial dynamic yield stress of 292 and a final of 670.5 Pa and it was rated initially 3 and finally 4. The G31-ST0.25 had an initial dynamic yield stress of 259 and a final of 940 Pa, and it was rated initially 3 and finally 4. The G32-HP0.3 had an initial dynamic yield stress of 135 and a final of 468, it was rated initially 3 and finally 4. Open time test is a measurement of the suitable time for printing with no disruption appearing in the printed layers. This time is also known as the printability window. The open time test is conducted to further determine the time during which the concrete will remain printable. The test was performed using the manual pump described earlier that has a nozzle with 3.7 cm width and 1 cm height, as shown in Fig. 18. This test was performed by printing 60 cm long parallel layers with the first layer printed after 30 min of water addition time. Successive layers were printed at 10-min intervals until a clear disruption happened to the printed layer at which the time was recorded as the open time for

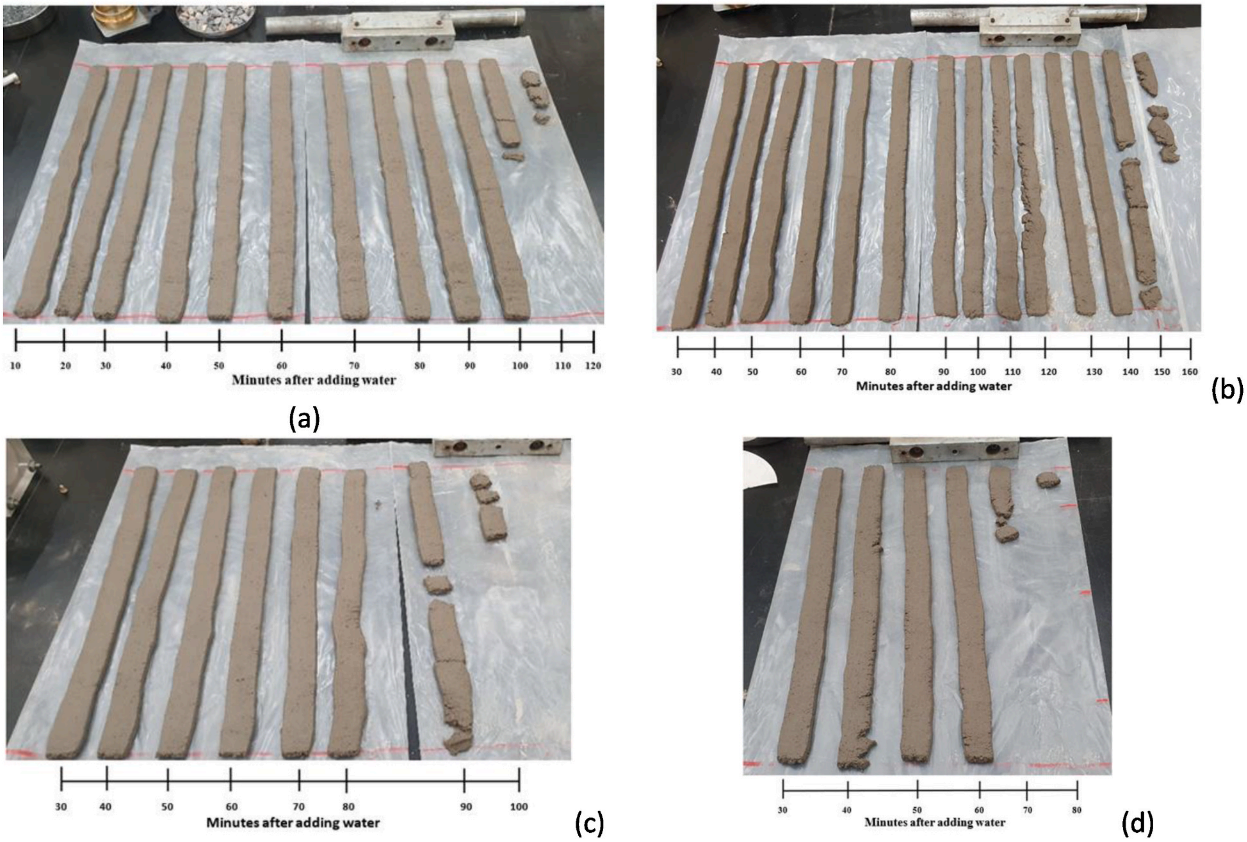

Fig. 18. Open time results: (a)0.25 % ST600, (b) 0.3 % HP6, (c) 0.3 FA and (d) 0.1MS.

Fig. 19. Photos of the large-scale gantry printer available in the ADU 3D Concrete Printing Research Lab.

printing. The results showed that the shortest open time was for the mix with G33-SF10 (60 min), followed by the mix with G11-FA30 (80 min), G31-ST0.25 (100 min) and then G32-HP0.3 (140 min), respectively. The fiber seems to provide a wider printability window compared to mixes without fibers.

4.4. Evaluation of developed mixes through large-scale printing

To verify the printability of the mixes in the printability box, selected mixes were picked within the printability box and were used in printing samples employing the large-scale gantry printer available in the ADU 3D Concrete Printing Research Lab established by the current authors at Abu Dhabi University. The mixing of concrete constituents was performed in accordance with the procedure described in the Tests and Methods section. The used gauntly printer shown in Fig. 19 utilizes a three-axis cartesian motion platform with three motors, each responsible for the movement in one of the x, y, or z directions. The printer's printing range is 1.6 m × 1.7 m x 1.8 m. The printing head is equipped with a screw extrusion system consisting of a coaxial single screw installed within a straight nozzle and controlled by a separate motor that has an adjustable extrusion rate. The nozzle is equipped with an exchangeable printing head with several opening sizes and shapes to choose from. In this research, a 3 cm circular printing head was used during the printing process for all the printed elements, which resulted in a 4 cm printed layer width. The layer height was chosen to be 2 cm for all the printed elements. The steady plane moving velocity when printing was taken to be 50 mm/s and the steady vertical moving velocity when printing was taken to be 5 mm/s. To optimize the printing time, the print path optimization option was switched on.

The researchers have intended to vary the printed shapes to be able to test the printability of the mixes with different geometries and complexities. Fig. 20 shows photos of 4 of the 3D printed concrete samples by the research team. Fig. 20a shows the photo of the printing of a rectangular bench with an internal arch and Fig. 20b shows the photo of the printing of a spiral shape demonstrating the printability of the picked mixes for simple shapes. Whereas Fig. 20c shows the photo of printing a garden bench, demonstrating the ability of the mix to print complex shapes and geometries. The research team elevated the printing challenge by successfully printing a twisted column as shown in Fig. 20d.

5. Conclusions

The experimental program aims to characterize the fresh properties and rheological properties of several 3D printed concrete mixes prepared with local material used in the construction industry in the United Arab Emirates (UAE). The effects of different mix constituents were evaluated and analyzed. To do that, several tests were carried out including: slump flow and rheology tests. The parameters that were investigated in this study are: fly ash replacement dosage, superplasticizer dosage, w/b ratio, silica fume replacement dosage and two types of fibers (ST600 and HP6). These parameters were varied one at a time to investigate their effects on the printability and buildability of the 3D printable mixes. The fresh and rheological properties were studied for up to 1 h, to evaluate the effects of elapsed time on the printability and buildability of the investigated 3DPC mixes. One of the key contributions of this paper is the proposed 3D printed concrete mixes rating evaluation procedure that has proven to be effective in evaluating and rating the extrudability and buildability of the studied mixes into four different ratings. The main advantage of this procedure is that it utilizes a manual grout gun, which is easy to implement on-site and can be used as a quality assurance tool for 3CPC mixes. In the course of this research, a printability chart was developed by plotting the dynamic yield stress against its corresponding plastic viscosity for each of the studied 3DPC mixes. The rating of each of the data points in the chart (based on the proposed rating procedure) was marked. Then, a printability box containing only the 3DPC mixes that were rated 4 (extrudable and buildable) was located. To evaluate the effectiveness of this printability box, several mixes from this box were selected and used in printing several samples with different geometries and complexities using the ADU large-scale gantry printer.

Below shows the summary of the key conclusions that can be drawn from the experimental program conducted during this research to study the effects of the varied parameters in the studied mixes.

- Shear thickening was observed for most 3DPC mixes.
- Final dynamic yield stress values were higher than the initial.
- The dynamic yield stress of the 3DPC mixes increased with higher replacement levels of fly ash (FA), fiber content, and silica fume, but decreased with higher water-to-binder ratio (w/b) and superplasticizer (SP) dosage.
- Fly ash (FA) improved the extrudability of 3DPC mixes with low w/b and high SP dosage at the initial stage. However, mixes with high w/b and low SP dosage containing FA require additional force for extrusion.
- The variation between initial and final dynamic yield stress values diminished with increasing w/b ratio and SP dosage, becoming nearly identical at the highest levels tested (w/b = 53 %, SP = 2 %).
- The dynamic yield stress of ST600 mixes increased significantly after 1 h when the fiber dosage exceeded 0.1 %. Caution is advised with higher dosages during prolonged printing, as they may hinder extrusion performance.
- Final plastic viscosity values were higher than the initial values.
- Slump flow values (D0, D15 and D25) decreased with the increase of the replacement dosage of FA and SF and the fiber contents. On the other hand, the slump flow values increased with the increase in w/b and SP dosage.
- Polynomial relationships were depicted between dynamic yield stress and slump flow values.
- No relationship was detected between slump flow and plastic viscosity.
- A printability box was established, indicating that 3DPC mixes with plastic viscosity values between 15 Pa s and 97 Pa s, and dynamic yield stress values between 400 Pa and 1500 Pa, are expected to exhibit adequate printability and were rated as level 4.

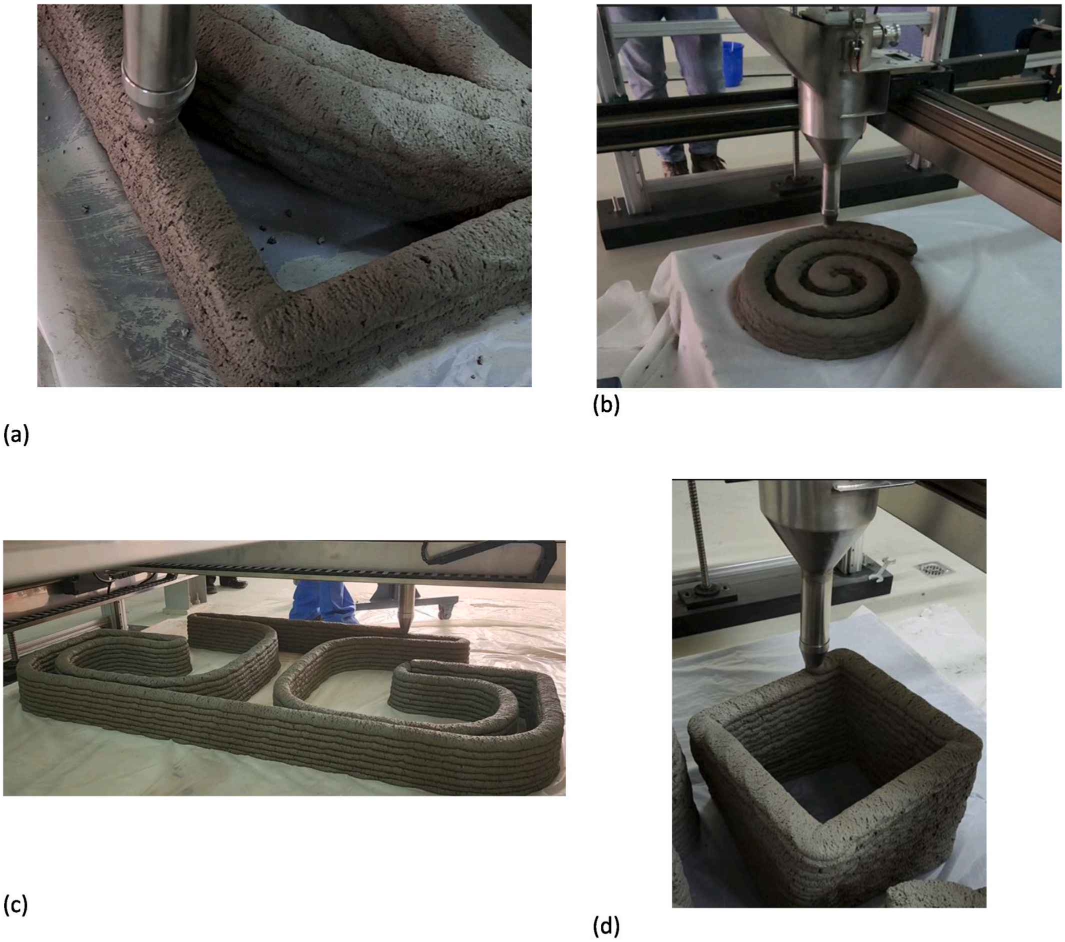

Fig. 20. Photos of the printing of large-scale elements using the developed 3DPC mixtures.

- The open time results for the selected mixes showed that the mix with SF has the shortest open time and the mix with HP6 fiber had the widest printability window.

It is worth noting that the above conclusions and developed relationships are pertinent to the investigated mixes in this study. To get a more generalized conclusion a comprehensive study incorporating a wider range of variables would be recommended.

List of Symbols and Abbreviations

Symbol/Abbreviation	Description	Unit
w/b	Water to binder ratio	dimensionless
SP	Superplasticizer	%by binder weight
FA	Fly ash	%replacement of binder
SF	Silica fume	%replacement of binder
3DPC	3D Printed concrete	–
τ_0	Dynamic Yield Stress	Pa
η	Plastic Viscosity	Pa·s
ST600	Synthetic Fiber Type 600	%by binder weight
HP6	Synthetic Fiber HP6	%by binder weight
D_0	Slump flow at 0 below	mm
D_{15}	Slump flow at 15 belows	mm
D_{25}	Slump flow at 25 belows	mm
Ω	the angular velocity of the outer cylinder	rad/s
T	Torque resistance	N.m
G	The yield value	N.m
H	viscosity factor	N.m.s
N	Rotational rate	Rev/s

CRediT authorship contribution statement

Reem Sabouni: Writing – review & editing, Visualization, Validation, Supervision, Resources, Project administration, Methodology, Investigation, Funding acquisition, Formal analysis, Conceptualization. **Samer Al Martini:** Writing – original draft, Visualization, Validation, Supervision, Resources, Project administration, Methodology, Investigation, Funding acquisition, Formal analysis, Conceptualization.

Declaration of competing interest

The authors declare the following financial interests/personal relationships which may be considered as potential competing interests: Samer Al Martini reports financial support was provided by Advanced Technology Research Council (ATRC) ASPIRE Grant. Samer Al Martini and Reem Sabouni has patent pending to Abu Dhabi University. If there are other authors, they declare that they have no known competing financial interests or personal relationships that could have appeared to influence the work reported in this paper.

Acknowledgments

The authors would like to acknowledge the support from the Advanced Technology Research Council (ATRC): the ASPIRE research grant (Grant No. AARE20-263), the Office of Research at Abu Dhabi University (Grant No. 19300556, Grant No. 19300649).

Data availability

Data will be made available on request.

References

[1] J. Burger, E. Lloret-Fritschi, F. Scotto, et al., Eggshell: ultra-thin three-dimensional printed formwork for concrete structures, 3D Print. Addit. Manuf. 7 (2) (2020).
[2] C. Zhang, Z. Hou, C. Chen, et al., Design of 3D printable concrete based on the relationship between flowability of cement paste and optimum aggregate content, Cem. Concr. Compos. 104 (2019).
[3] A. Kazaz, S. Ulubeyli, T. Acikara, et al., Factors affecting labor productivity: perspectives of craft workers, Procedia Eng. (2016).
[4] R. Duballet, O. Baverel, J. Dirrenberger, Classification of building systems for concrete 3D printing, Autom. ConStruct. 83 (2017).
[5] L. Loizou, K. Barati, X. Shen, et al., Quantifying advantages of modular construction: waste generation, Buildings 11 (12) (2021).
[6] M. Yeheyis, K. Hewage, M.S. Alam, et al., An overview of construction and demolition waste management in Canada: a lifecycle analysis approach to sustainability, Clean Technol. Environ. Policy (2013).
[7] J. Kim, A.M. Grabiec, A. Ubysz, An experimental Study on structural concrete containing recycled aggregates and powder from construction and demolition waste, Materials 15 (7) (2022).
[8] F. Bos, R. Wolfs, Z. Ahmed, et al., Additive manufacturing of concrete in construction: potentials and challenges of 3D concrete printing, Virtual Phys. Prototyp. 11 (3) (2016).
[9] H. Nasir, H. Ahmed, C. Haas, et al., An analysis of construction productivity differences between Canada and the United States, Construct. Manag. Econ. 32 (6) (2014).
[10] T. Bock, The future of construction automation: technological disruption and the upcoming ubiquity of robotics, Autom. ConStruct. 59 (2015).
[11] F. Lyu, D. Zhao, X. Hou, et al., Overview of the development of 3D-printing concrete: a review, Appl. Sci. (2021).
[12] J. De Vlieger, L. Boehme, J. Blaakmeer, et al., Buildability assessment of mortar with fine recycled aggregates for 3D printing, Constr. Build. Mater. 367 (2023).
[13] W. Cui, T. Wang, X. Chen, et al., Study of 3D printed concrete with low-carbon cementitious materials based on its rheological properties and mechanical performances, J Sustain Cem Based Mater 12 (7) (2023).
[14] R. Sabouni, H.R. Abdulhameed, Optimization of sustainable concrete mixes containing binary and ternary blends, Key Eng. Mater. (2020).
[15] Z. Li, L. Wang, G. Ma, Method for the enhancement of buildability and bending resistance of 3D printable tailing mortar, Int J Concr Struct Mater. 12 (1) (2018).
[16] G. Duarte, J.P. Duarte, A. Memari, et al., Towards a model for structural performance in concrete printing based on buildability and toolpath design, J. Build. Eng. 69 (2023).
[17] Q. Deng, S. Zou, Y. Xi, et al., Development and characteristic of 3D-Printable mortar with waste glass powder, Buildings 13 (6) (2023).
[18] M.T. Mollah, R. Comminal, M.P. Serdeczny, et al., Computational analysis of yield stress buildup and stability of deposited layers in material extrusion additive manufacturing, Addit. Manuf. 71 (2023).
[19] G.H. Andrew Ting, T.K. Noel Quah, J.H. Lim, et al., Extrudable region parametrical study of 3D printable concrete using recycled glass concrete, J. Build. Eng. 50 (2022).
[20] J. Xiao, S. Hou, Z. Duan, et al., Rheology of 3D printable concrete prepared by secondary mixing of ready-mix concrete, Cem. Concr. Compos. 138 (2023).
[21] S. Paritala, K.K. Singaram, I. Bathina, et al., Rheology and Pumpability of Mix Suitable for Extrusion-based Concrete 3D Printing – a Review, Constr Build Mater, 2023.
[22] M. Dahlenburg, C.M. Hechtl, C. Matthaus, et al., 3D-Concrete printing-graded concrete extrusion. Proceedings - 2022 3rd International Conference on Computation, Automation and Knowledge Management, ICCAKM 2022, 2022.
[23] A.R. Arunothayan, B. Nematollahi, K.H. Khayat, et al., Rheological characterization of ultra-high performance concrete for 3D printing, Cem. Concr. Compos. 136 (2023).
[24] Y. Zhao, G. Yang, L. Zhu, et al., Effects of rheological properties and printing speed on molding accuracy of 3D printing basalt fiber cementitious materials, J. Mater. Res. Technol. (2022).
[25] A.H.M. Hosseiny, A. Najafi, G. Khalaj, Investigation of CaO/MgO on the formation of Anorthite, Diopside, Wollastonite and Gehlenite phases in the fabrication of fast firing ceramic tiles, Constr. Build. Mater. 394 (2023).
[26] O. Fakhimi, A. Najafi, G. Khalaj, A facile rout to obtain Al2O3 nanopowder via recycling aluminum cans by sol-gel method, Mater. Res. Express 7 (4) (2020).

[27] M. Rahmani-Azad, A. Najafi, N. Rahmani-Azad, et al., Improvement of ZrB2 nanopowder synthesis by sol-gel method via zirconium alkoxide/boric acid precursors, J. Sol. Gel Sci. Technol. 103 (1) (2022).
[28] A. Hassan, T. Alomayri, M.F. Noaman, et al., 3D Printed Concrete for Sustainable Construction: a Review of Mechanical Properties and Environmental Impact, Archives of Computational Methods in Engineering. Springer Science and Business Media B.V., 2025, pp. 2713–2743.
[29] G.M. Moelich, P.J. Kruger, R. Combrinck, A plastic shrinkage cracking risk model for 3D printed concrete exposed to different environments, Cem. Concr. Compos. 130 (2022).
[30] M. Kaszyńska, M. Hoffmann, S. Skibicki, et al., Evaluation of suitability for 3D printing of high performance concretes. MATEC Web of Conferences, 2018.
[31] G.M. Moelich, P.J. Kruger, R. Combrinck, Mitigating early age cracking in 3D printed concrete using fibres, superabsorbent polymers, shrinkage reducing admixtures, B-CSA cement and curing measures, Cement Concr. Res. (2022) 159.
[32] H. Alghamdi, N. Neithalath, Synthesis and characterization of 3D-printable geopolymeric foams for thermally efficient building envelope materials, Cem. Concr. Compos. 104 (2019).
[33] L. Yang, Y. Gao, H. Chen, et al., Three-dimensional concrete printing technology from a rheology perspective: a review, Adv. Cement Res. 36 (12) (2024) 567–586.
[34] S. Chen, S.B. Khan, N. Li, et al., In-depth analysis of sintering, exposure time, and layer height (um) in LRS 3D printed devices with DLP, J. Manuf. Process. 133 (2025) 576–591.
[35] A.C.M. Soares, H. Costa, R. do Carmo, et al., Comprehensive Design Methodology for 3D Printing Mortars, 401, Constr Build Mater, 2023.
[36] A.S. Natanzi, C. McNally, Characterising Concrete Mixes for 3D Printing, RILEM Bookseries, 2020.
[37] B. Panda, M.J. Tan, Rheological behavior of high volume fly ash mixtures containing micro silica for digital construction application, Mater. Lett. 237 (2019).
[38] M. Nehdi, S. Ai-Martini, Coupled effects of high temperature, prolonged mixing time, and chemical admixtures on rheology of fresh concrete, ACI Mater. J. 106 (3) (2009).
[39] S. Al Martini, A. Khartabil, N. Neithalath, Rheological properties of recycled aggregate concrete incorporating supplementary cementitious materials, ACI Mater. J. 118 (6) (2021).
[40] N. Roussel, Rheological requirements for printable concretes, Cement Concr. Res. (2018).
[41] D. Kaplan, F. De Larrard, T. Sedran, Design of concrete pumping circuit, ACI Mater. J. 102 (2) (2005).
[42] D. Feys, R. Verhoeven, G. De Schutter, Fresh self compacting concrete, a shear thickening material, Cement Concr. Res. 38 (7) (2008).
[43] M. Choi, N. Roussel, Y. Kim, et al., Lubrication layer properties during concrete pumping, Cement Concr. Res. 45 (1) (2013).
[44] S.A. Martini, A. Khartabil, M.L. Nehdi, Estimating rheological properties of superplasticized cement paste at high temperature and prolonged mixing using various rheological models and oscillatory rheology, ACI Mater. J. 118 (6) (2021).
[45] Z. Pan, H. De Cagny, B. Weber, et al., S -shaped flow curves of shear thickening suspensions: direct observation of frictional rheology, Phys. Rev. E - Stat. Nonlinear Soft Matter Phys. 92 (3) (2015).
[46] L. Struble, G.K. Sun, Viscosity of Portland cement paste as a function of concentration, Adv. Cement Base Mater. 2 (2) (1995).
[47] Y. Li, A.K.H. Kwan, Ternary blending of cement with fly ash microsphere and condensed silica fume to improve the performance of mortar, Cem. Concr. Compos. 49 (2014).
[48] T. Mezger, Applied rheology. Anton Paar, 2014.
[49] N. Roussel, A thixotropy model for fresh fluid concretes: theory, validation and applications, Cement Concr. Res. 36 (10) (2006).
[50] S. Al-Martini, M.I. Al-Khatib, Rheology of self-consolidating concrete in hot weather conditions, in: Proceedings of Institution of Civil Engineers: Construction Materials, 2020, 173(5).
[51] M. Nehdi, S. Al Martini, Effect of temperature on oscillatory shear behavior of Portland cement paste incorporating chemical admixtures, J. Mater. Civ. Eng. 19 (12) (2007).
[52] D. Marchon, S. Kawashima, H. Bessaies-Bey, et al., Hydration and rheology control of concrete for digital fabrication: potential admixtures and cement chemistry, Cement Concr. Res. (2018).
[53] S. Ketel, G. Falzone, B. Wang, et al., A printability index for linking slurry rheology to the geometrical attributes of 3D-printed components, Cem. Concr. Compos. (2019) 101.
[54] V.N. Nerella, M. Näther, A. Iqbal, et al., Inline quantification of extrudability of cementitious materials for digital construction, Cem. Concr. Compos. 95 (2019).
[55] T.T. Le, S.A. Austin, S. Lim, et al., Mix design and fresh properties for high-performance printing concrete, Materials and Structures/Materiaux et Constructions 45 (8) (2012).
[56] V.N. Nerella, M.A.B. Beigh, S. Fataei, et al., Strain-based approach for measuring structural build-up of cement pastes in the context of digital construction, Cement Concr. Res. 115 (2019).
[57] G. Beersaerts, T. Hertel, S. Lucas, et al., Promoting the use of Fe-rich slag in construction: development of a hybrid binder for 3D printing, Cem. Concr. Compos. 138 (2023).
[58] M. Hambach, D. Volkmer, Properties of 3D-printed fiber-reinforced Portland cement paste, Cem. Concr. Compos. 79 (2017).
[59] L.J. Struble, C.T. Chen, Effect of continuous agitation on concrete rheology, J. ASTM Int. (JAI) 2 (9) (2005).
[60] S. Al-Martini, M. Nehdi, Effect of chemical admixtures on rheology of cement paste at high temperature, J. ASTM Int. (JAI) 4 (3) (2007).
[61] H. Mori, Y. Tanigawa, Flow simulation of fresh concrete subjected to vibration, Mag. Concr. Res. 42 (153) (1990).